Dinakar Sagapuram
Department of Industrial and Systems Engineering,
Texas A&M University,
College Station, TX 77843
e-mail: dinakar@tamu.edu

Anirudh Udupa
Center for Materials Processing and Tribology,
Purdue University,
West Lafayette, IN 47907-2023
e-mail: audupa@purdue.edu

Koushik Viswanathan
Department of Mechanical Engineering,
Indian Institute of Science,
Bangalore 560012, India
e-mail: koushik@iisc.ac.in

James B. Mann
Department of Mechanical Engineering,
University of West Florida,
Pensacola, FL 32514
e-mail: jbmann@uwf.edu

Rachid M'Saoubi
R&D Material and Technology Development,
Seco Tools AB,
Fagersta 737 82, Sweden
e-mail: rachid.msaoubi@secotools.com

Tatsuya Sugihara
Department of Mechanical Engineering,
Osaka University,
Suita, Osaka 565-0871, Japan
e-mail: t-sugihara@mech.eng.osaka-u.ac.jp

Srinivasan Chandrasekar[1]
Center for Materials Processing and Tribology,
Purdue University,
West Lafayette, IN 47907
e-mail: chandy@purdue.edu

On the Cutting of Metals: A Mechanics Viewpoint

The mechanics of large-strain deformation in cutting of metals is discussed, primarily from viewpoint of recent developments in in situ analysis of plastic flow and microstructure characterization. It is shown that a broad range of deformation parameters can be accessed in chip formation—strains of 1–10, strain rates of 10–10^5/s, and temperatures up to 0.7T_m—and controlled. This range is far wider than achievable by any other single-stage, severe plastic deformation (SPD) process. The resulting extreme deformation conditions produce a rich variety of microstructures in the chip. Four principal types of chip formation—continuous, shear-localized, segmented, and mushroom-type—as elucidated first by Nakayama (1974, "The Formation of 'Saw-Toothed Chip' in Metal Cutting," Proceedings of International Conference on Production Engineering, Tokyo, pp. 572–577) are utilized to emphasize the diverse plastic flow phenomena, especially unsteady deformation modes that prevail in cutting. These chip types are intimately connected with the underlying flow, each arising from a distinct mode and triggered by an instability phenomenon. The role of plastic flow instabilities such as shear banding, buckling, and fracture in mediating unsteady flow modes is expounded, along with consequences of the flow modes and chip types for the cutting. Sinuous flow is shown to be the reason why gummy (highly strain-hardening) metals, although relatively soft, are so difficult to cut. Synthesizing the various observations, a hypothesis is put forth that it is the stability of flow modes that determines the mechanics of cutting. This leads to a flow-stability phase diagram that could provide a framework for predicting chip types and process attributes. [DOI: 10.1115/1.4047869]

Keywords: advanced materials and processing, bulk deformation processes (e.g., extrusion, forging, wire drawing, etc.), machining processes

1 Introduction

Machining or cutting is a manufacturing process that is commonly used to produce finished components of desired shape, size, and surface finish. The cutting process utilizes single or multiple point cutting tools with well-defined geometry to remove unwanted material from the workpiece in the form of chips. Although cutting and similar material removal processes have been in use in some form or another since antiquity, it is only during the latter half of the 19th century that systematic research was initiated to place the subject on a sound scientific basis. Excellent reviews of early work in the field, including historical perspectives, have been presented by Mullins and Shaw [1]. The modern era of research into cutting can be traced to the work of Ernst and Merchant [2], Ernst [3], and Shaw [4–6] (circa 1940–1950) which sought to study the material removal process from a mechanics-materials perspective. This work recognized that the mechanics of chip formation, even though the chip is generally an unwanted by-product of cutting, is the key to determining forces, energy, deformation, and microstructure in machining. In the last 30 years, with the advent of a variety of high-resolution microscopy methods and surface analysis tools, along with advances in numerical analysis methods, cutting research has evolved with greater emphasis on the materials-mechanics aspects of large-strain deformation, and related modeling, both from a continuum and a microstructure-based perspective.

The present paper is structured mainly around expositing the key role of large-strain deformation in cutting of metals, primarily from viewpoint of recent developments in in situ analysis of plastic flow, and microstructure characterization; complemented by discussion of classical work. The topics covered include nature of large-strain plastic deformation in cutting; influence of this deformation on material microstructure and properties; how can the cutting-deformation be varied or controlled; and what governs or determines the nature (type) of chip formation. We conclude with a summary of the state-of-the-art as viewed through the mechanics-materials prism and potential topics for further research.

2 Mechanics of Continuous Chip Formation: Type 2 Chip With Laminar Flow

An instructive place to begin the discussion of large-strain deformation in metal cutting is with the analysis of mechanics of

[1]Corresponding author.

Manuscript received November 27, 2019; final manuscript received July 10, 2020; published online September 8, 2020. Assoc. Editor: Albert Shih.

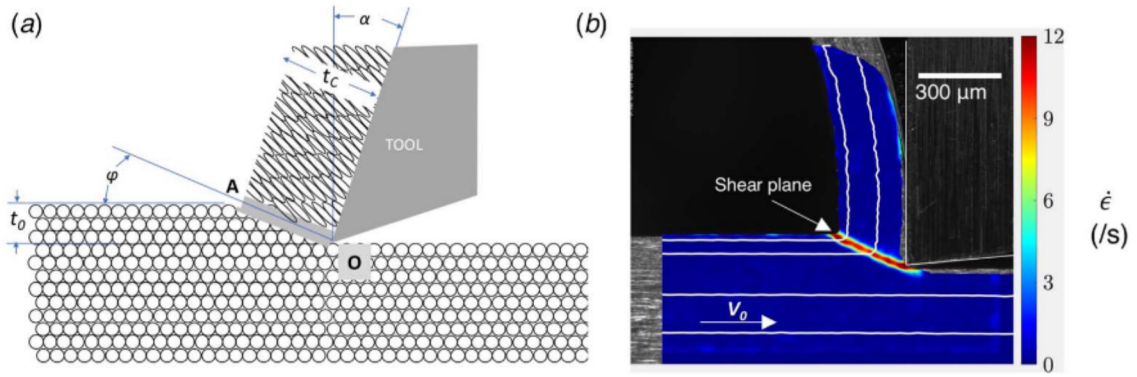

Fig. 1 Shear plane model of cutting. (*a*) Schematic illustrating mechanism of formation of continuous (Type 2) chip and resulting distortion of grain structure. (*b*) Imaging of material flow in pre-strained Cu showing uniform deformation with smooth streaklines, and a highly confined deformation zone (shear plane). Background color map is strain rate field. $V_0 = 1$ mm/s.

continuous chip formation—the so-called Type 2 chip (Fig. 1)—carried out by Merchant [7,8] and Piispanen [9]. This type of chip is common when cutting metal alloys of moderate ductility such as copper, aluminum, and mild steel especially in an initially pre-strained condition. Based on metallographic observations [2,7], the well-known shear plane model of deformation was proposed for the formation of this Type 2 chip under conditions of plane-strain —the framework usually preferred for analysis of mechanics of cutting. Figure 1(*a*) shows a schematic of this model wherein the chip develops by a process of intense (simple) shear that is confined to a narrow region (primary deformation zone (PDZ)), idealized as a shear plane OA inclined at angle ϕ (shear angle) to the cutting velocity direction. Since the geometry of the cutting for Type 2 chip is essentially determined by the shear plane orientation, various hypotheses/models have been put forth for analytically predicting the angle ϕ—for example, minimum energy consumption [8] and plane of maximum shear stress [9] or via slip-line field analysis [10–12].

Figure 1(*b*) shows one frame from a high-speed image sequence of Type 2 chip formation in cutting of pre-deformed copper (strain ~1.5). This picture of the chip formation and associated deformation confirms many of the characteristics depicted in Fig. 1(*a*). The strain rate field (color) that represents the deformation zone is superimposed onto this image; its confined nature highlights the shear plane. The streaklines of flow, also superimposed in Fig. 1(*b*) and shown as white lines, are uniform and smooth indicating homogeneous steady deformation; we shall refer to this type of flow as laminar, using an analogy from fluid mechanics (Note: A streakline is the locus of all material points passing through a fixed spatial location during deformation). Such imaging observations, dating back even to the 1940s using cinematography, as well as records of deformation of grids inscribed on the workpiece, have largely confirmed the shear plane model, or more broadly the shear zone model (finite deformation zone thickness) [7,11,13–15] picture of Type 2 chip formation. The existence of shear plane/zone deformation has also been validated by numerical simulations [16–20]. In the present review, which is concerned primarily with the large-strain deformation aspects of cutting, we will not distinguish between the shear plane and shear zone descriptions, since both give a very similar picture of the deformation.

Based on the shear plane model, Merchant derived kinematic and force relationships relating various velocities and force components in terms of the process parameters: cutting speed V_0, tool rake angle α, undeformed chip thickness t_0, and thickness of the cut (deformed) chip t_c. However, of more importance for this review are the resulting expressions derived for the cutting ratio (r), shear plane angle (ϕ), shear strain (γ), and strain rate ($\dot{\gamma}$) in the deformation zone:

$$r = \frac{t_0}{t_c} = \frac{\sin(\phi)}{\cos(\phi - \alpha)} \tag{1}$$

$$\phi = \tan^{-1}\left[\frac{r\cos(\alpha)}{1 - r\sin(\alpha)}\right] \tag{2}$$

$$\gamma = \frac{\cos(\alpha)}{(\sin(\phi)\cos(\phi - \alpha))} = \cot(\phi) + \tan(\phi - \alpha) \tag{3}$$

If the shear plane is assumed to be a zone of finite but small thickness (ΔX), then the average strain rate in this zone is obtained as follows:

$$\dot{\gamma} = \gamma \cdot \frac{V_0}{\Delta X} \tag{4}$$

The von Mises effective strain for the plane-strain cutting is given by $\varepsilon = \frac{\gamma}{\sqrt{3}}$. An alternative expression for the strain [21–23] that follows directly from Eqs. (1)–(3) above is

$$\gamma = \frac{\lambda}{\cos(\alpha)} + \frac{1}{\lambda\cos(\alpha)} - 2\tan(\alpha) \tag{5}$$

where $\lambda = \frac{1}{r}$ is the chip-thickness ratio. Equation (5) has the advantage that the strain is directly related to measurable parameters, viz., t_c, t_0 and α, whereas Eq. (3) for strain requires an intermediate step of estimating ϕ from chip thickness measurements.

It is useful to examine the magnitudes of strain and strain rate in the shear plane region. For example, using the process parameters corresponding to cutting of hardened Cu in Fig. 1(*b*) ($\lambda \sim 2$, $\alpha = 0$ deg), the estimated shear strain γ is ~2.5 and the effective strain ε is ~1.45. Likewise, if we consider cutting of annealed Cu where $\lambda \sim 12$ (for $\alpha = 0$ deg), then assuming that the shear plane model provides an adequate description of the flow, we get ε as large as ~7. Estimates such as these show that the effective strains in metal cutting are quite large, typically in the range of 1–10. Similarly, the strain rates in the deformation zone have been estimated based on optical metallography characterization of the deformation zone thickness and Eq. (4) [13,14,24–28]. These show that like the strains, strain rates too are extreme, typically $10–10^5$/s for cutting speeds in the range of a few millimeters per second to a few meter per second. The higher end of this strain rate range overlaps with that prevailing in materials subjected to shock deformation. These strain and strain rate estimates have been also confirmed/validated by grid-deformation [11,13,24,29] and visioplasticity analyses [11]; as well as, more recently, by particle image velocimetry (PIV) or digital image correlation (DIC) analyses of high-speed images of material flow in the deformation zone, such as presented in Fig. 1(*b*) [28,30,31].

An important consequence of this intense deformation in the PDZ is the changes in the microstructural state of the metal as it traverses the shear plane. This is seen in the optical micrograph shown in

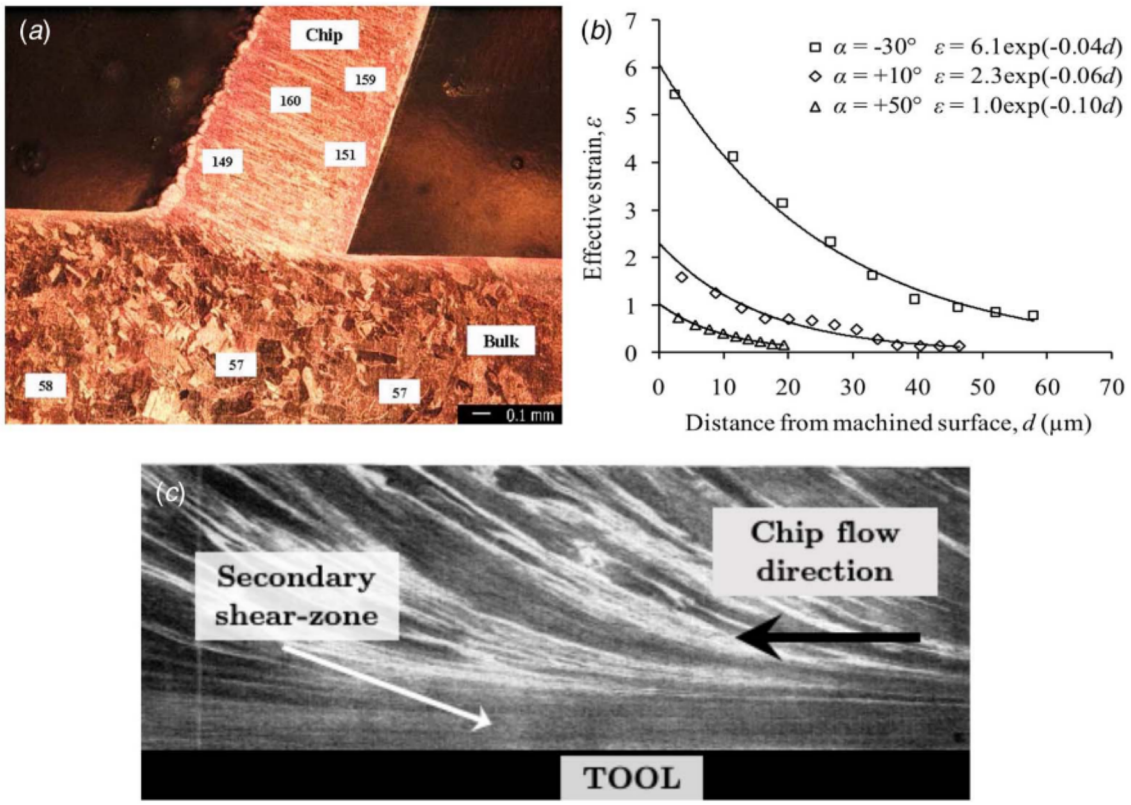

Fig. 2 Large-strain deformation, flow-lines, and microstructure in Type 2 chip: (*a*) Cutting of annealed Cu showing grain refinement in shear zone and increase in material hardness. The Vickers hardness values in the bulk and chip are superimposed [28]. (*b*) Strain distribution on machined surface/subsurface of 260 brass derived from PIV analysis of material flow [32]. $t_0 = 150$ μm. (c) Material flow pattern near tool–chip interface (secondary deformation zone) in cutting of steel highlighting severity of (secondary) deformation arising from friction [25]. The shear strain at this interface is >25 based on flow-line analysis.

Fig. 2(*a*) for annealed Cu, derived from quick-stop observations of the cutting process. The microstructure change is obvious from the initial grain structure of the workpiece material (grain size 50–100 μm) being replaced by a flow-line type morphology in the chip. The transition of microstructure is also fairly sharp, occurring over a narrow region, thereby validating the shear plane/shear zone models that have been proposed [4,8,9]. It should be noted that the lack of visibility of clear grain structure in the chip does not mean that the material has become amorphous; it is just indicative of the fact that the grain size is so fine (<1 μm), as to be below the optical resolution limit. The images in Fig. 3, obtained using transmission electron microscopy (TEM), illustrate the ultrafine-grained (UFG) structure of machined chips produced from commercially pure Al and Ti. The chip microstructure in both the cases is composed of micron/submicron-sized grains with few internal dislocations. This type of UFG microstructure has been observed in various alloy systems and is concomitant with the chip hardness being two- to threefold times that of the bulk (workpiece) material hardness [23,33–38]; also see the hardness numbers marked in Fig. 2(*a*) which show that the chip is approximately three times as hard as the initial Cu workpiece. This microstructure refinement to the sub-micron scales parallels what has been observed in the pioneering studies of large-strain deformation of metals (via repeated wire drawing) by Embury and Fisher [39], and Langford and

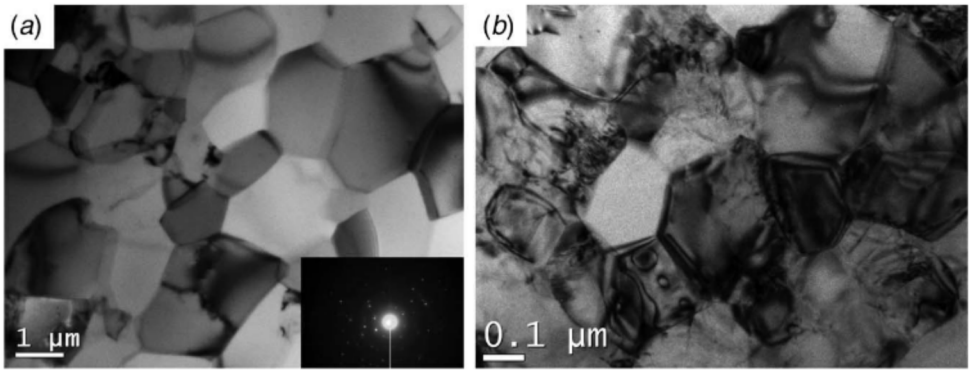

Fig. 3 TEM micrographs showing UFG/nanocrystalline microstructures in machining chips: (*a*) pure aluminum ($\gamma = 17$, $d\gamma/dt \sim 100/s$) and (*b*) commercially pure titanium, grade 2 ($\gamma = 3$, $d\gamma/dt \sim 2500/s$)

Cohen [40]. However, in the case of cutting, this microstructure transformation (across the PDZ) is effected in a single step.

Another inference from observations such as Fig. 2(*a*) and high-speed imaging of flow is that the chip deformation field is also inherited on the machined surface. Recent quantitative measurements of machined surface deformation using PIV analysis (see Fig. 2(*b*)) show that the residual plastic deformation extends into the subsurface, up to a few tens of microns, with strain levels in the near-surface region being large and close to the chip strain. Consequently, the machined surface microstructure is expected (and in fact confirmed [32]) to mirror that of the chip. It is seen from Fig. 2(*b*) that the rake angle has a major influence on the machined surface strain, this strain increasing with decreasing rake angle. A third region in machining chip formation that experiences considerable deformation, perhaps even more severe than in the PDZ or machined surface, is the secondary deformation zone (SDZ) adjoining the tool–chip contact [25,41], see flow-line pattern in Fig. 2(*c*). The straining in the SDZ arises from the severe friction conditions at the tool–chip contact and is typically manifested as a thin zone of intense shear on the underside of the chip (Fig. 2(*c*)). Its resemblance to a "plastic boundary layer" has also been discussed [42,43]. An estimate of the strain in this region, obtained from analysis of curvature of the flow lines [25,44], gives values >25. More examples of this intense secondary deformation can be found in the excellent optical micrographs presented by Zorev and Trent [25,41].

Equations (1)–(5) show that the strain and strain rates in the primary deformation zone can be systematically varied over a wide range—strains of 0.5 to 10, strain rates of 10–10^5/s—by controlling the cutting process parameters (α, V_0, etc.). Note that this range is much wider than is possible in any other single-stage deformation process or materials test. This together with the highly confined (simple shear) nature of the deformation (Fig. 1) suggests that the process of chip formation could be used as a materials test for measuring mechanical properties of metal alloys at large strains and high strain rates, as pointed out by some of the pioneers of metal cutting mechanics including Shaw [5], Drucker [45], and Thomsen and Lapsley [46]. Similarly, chip formation offers unique capability for studying microstructural changes (e.g., grain refinement, dislocation substructures) arising from severe plastic deformation (SPD) [33]. Complete studies of microstructure evolution and associated mechanical strength properties in metals over a wide strain/strain rate/temperature parameter space—enabled by machining simple shear deformation—can be found in Refs. [23,33–38,47]. These studies have shown that the deformation conditions in machining can be varied to study (and produce) a diverse variety of highly refined microstructures over and beyond the equiaxed UFG microstructures shown in Fig. 3, including nanotwinned [37,48], multi-phase UFG [34], and bimodal structures [33]. In this context, it is worth noting the extraordinary interest these latter unconventional microstructures have received in recent years because of their unusual property combinations of high strength, thermal stability, and ductility [48–53]. Moreover, since microstructural changes in machining are not just confined to the chip but are also inherited on the machined workpiece surface, these observations suggest new opportunities for using machining to engineer surfaces with interesting microstructures [32].

At this juncture, we should also draw attention to an important difference between the deformation geometry in metal cutting and that of bulk metal forming processes such as extrusion, rolling, and drawing. In the forming processes, the geometry of the deformation, and hence the strain, are defined a priori, that is the shape and size of the workpiece material at inlet and exit of the die are predefined. Whereas in metal cutting, the deformation is unconstrained and, the thickness of the "deformed chip" is an output of the process, thus making any deformation analysis a free-boundary value problem in the theory of plasticity. It is this difference, with associated proximity of the deformation zone to the free surface, that makes the mechanics of cutting particularly difficult to model. And it is for this reason Merchant hypothesized that the orientation of the shear plane is determined by an extremum principle—total energy dissipated being a minimum [8]. This proximity to the free surface and the resulting unconstrained deformation spawn a diverse and rich variety of flow modes, both uniform (e.g., Fig. 1) and non-uniform or unsteady (e.g., shear bands). As a result, the cutting framework is particularly well-suited also for studying plastic flow modes and flow instabilities in large-strain deformation, both quantitatively and from a phenomenological perspective (see discussion in Sec. 8).

3 Overview of Chip Types and Flow Modes

Type 2 continuous chip with underlying homogeneous uniform deformation (laminar flow) (Fig. 1) is by no means the only type of chip morphology, nor is it the norm, in cutting of metals. Even a cursory examination of chips collected from a machine shop, wherein metals like Cu, Al, Ti and steels are machined, will lead one to conclude that there are many chip morphologies (types)—indeed, perhaps even as many types as there are alloys. But a more careful examination [41,54,55] will show that there are but a handful of principal chip morphologies. Nakayama, in particular, recognized this and classified continuous chips into four types, as shown in the schematic (chip line drawings) of Fig. 4 [58]. (This classification, including the Type number, is somewhat different from that due to Ernst and Merchant [2]; the latter also includes chips such as connected with built-up edge formation which are not considered here). For reference, chips from cutting experiments that correspond to these morphologies are also shown alongside the schematics in Fig. 4. Note here that Type 2 chip discussed earlier is the one depicted in the top right of the figure; the schematic of this chip is shown with some waviness that sometimes arises from variation in undeformed chip thickness. The chip types of Fig. 4 are also quite important for workpiece surface integrity since evidence suggests the surface deformation state mirrors that of the chip. We will utilize this chip morphology classification, since each of these chip types can then be uniquely associated with (arise from) a fundamental mesoscale, plastic flow mode. As a result, the chip formation and morphology can be discussed in a rigorous plasticity framework that provides new insights not only into the cutting process but more broadly into plastic flow phenomena in metals, especially the underlying relationship with material microstructure/state and deformation conditions.

When cutting ductile (polycrystalline) metals such as aluminum, copper, and single-phase brass, in the soft annealed condition, the chip that forms is usually very thick (~15–20), with characteristic wrinkled mushroom-like features and "cracks" on its back surface [41,58–60]. This is Type 1 chip (Fig. 4, top left), also seen in cutting of other highly strain-hardening metals like tantalum, niobium, and stainless steels, at low-to-medium speeds (note that at higher speeds, for example in stainless steels, the flow transitions to one dominated by shear banding). This chip formation is characterized by unusually large cutting forces—unusual in that the forces are high even though the metals being cut are relatively soft. The large forces are consistent with the extreme, often 15–20 fold, thickening of the chip as it traverses the deformation zone; this thickening is indicative of extreme straining in the shear plane model. Another distinguishing feature of this type of chip formation is the occurrence of a thick severely strained layer (~t_0) on the workpiece surface with extensive side flow of the material. In view of these characteristics, these highly strain-hardening, but mostly soft, metals are quite difficult to cut, also earning them the moniker "gummy" in machine-shop lore [61]. In contrast, when the same metals are cut in an initially pre-worked (pre-strained) condition, the chip is much thinner (~2–3t_0, and of Type 2), the forces significantly lower (by a factor of 2–3) and the strained workpiece layer, much less thick. The thick Type 1 chip has traditionally been explained using the shear zone model, by postulating a broad deformation zone that has spread out into the workpiece, a small effective shear plane angle (~0 deg), and non-uniform deformation. The wrinkles

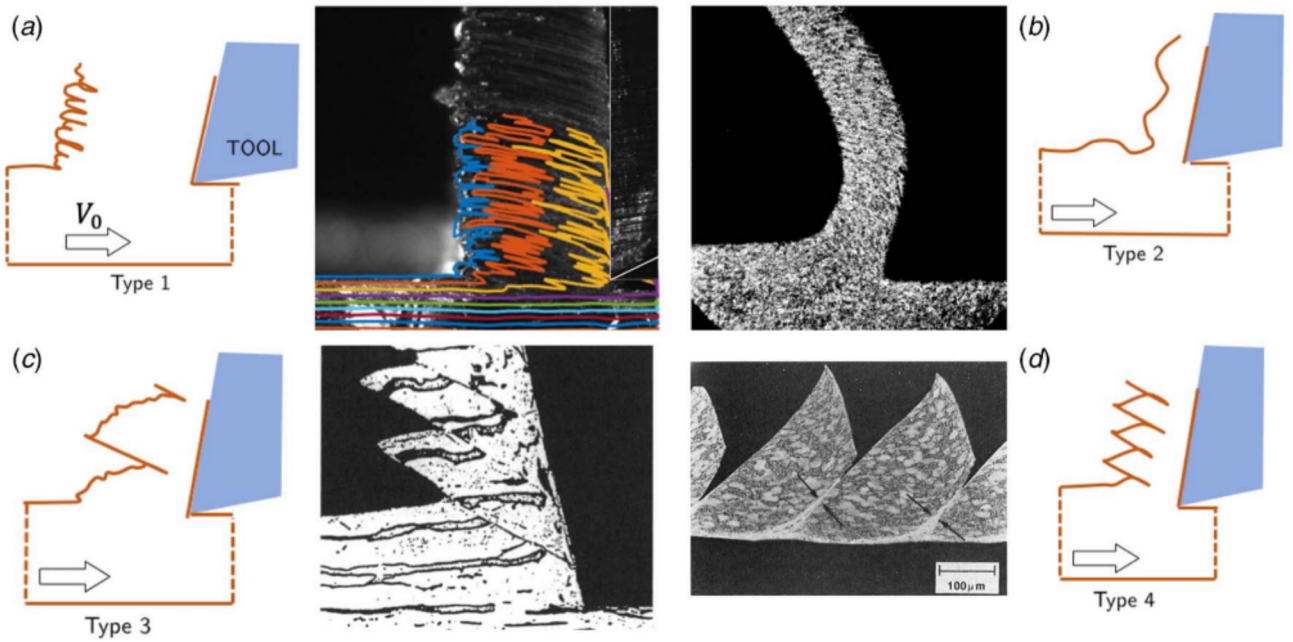

Fig. 4 Schematic and optical micrographs of the four principal chip types according to Nakayama's classification: (*a*) Type 1 chip observed in cutting of soft and highly strain-hardening metals, (*b*) Type 2 chip from laminar flow [2], (*c*) segmented Type 3 chip [56] (Reprinted with permission from Elsevier © 1993), and (*d*) shear-localized Type 4 chip [57].

and mushroom-like features have been attributed to "the non-uniform deformation (a fact that is obvious from examination of the chip flow lines) and crack corresponding to the non-uniform nature of polycrystalline metal" [58]. It is only recently that the role of unsteady flow in formation of Type 1 chip has been explicitly recognized and characterized [62,63], including the relation between its morphological features and the underlying flow attributes.

The most recognized examples of chip morphologies arising from unsteady flow are those that form by segmentation [64,65] —Type 3 chip; or via shear banding/localization [64,66–68]— Type 4 chip, see bottom row of Fig. 4. The former occurs with metals of low-to-moderate workability such as hard steels, and Mg and Zn; and even with moderately ductile metals (e.g., 2-phase brass) when cutting with a negative rake angle tool. The shear-localized Type 4 chip is most prominent in cutting of metals with low thermal conductivity/diffusivity, e.g., Ti and Ni alloys [57,64,67]. In certain instances, there is evidence suggesting that the shear banding and segmentation are linked with the former preceding the latter [69,70]. The morphologies of both Type 3 and Type 4 chips are broadly similar with both of them showing a saw-tooth or serrated appearance (Fig. 4). But, as will be seen later, the underlying deformation mechanics is quite different, with flow localization in shear banding occurring by intense adiabatic (catastrophic) shear in thin zones wherein the strains are extreme ~10–25 [4,64,67]; whereas with the segmented Type 3 chip, the serrated appearance arises from periodic fracture at the free surface, with the (non-uniform) strains in the chip restricted to ~2–3.

A noteworthy point to which we will return, especially when discussing why different chip types arise, is that the chip morphology is determined by the underlying flow mode. This is to be expected since deformation in cutting is unconstrained, occurring in close proximity to a free surface—providing a degree of freedom which allows for prevalence of different flow types. Various discontinuous chip types [71–74], i.e., broken chips, such as seen when machining cast iron and other cast alloys with poor microstructure integrity (e.g., leaded brass) or materials of low-workability (e.g., Mg) are but extreme examples of Type 3 morphology.

We shall now discuss in greater detail the chips with irregular morphology and the underlying unsteady flow patterns and plastic flow instabilities.

4 Type 3 Chip and Segmented Flow

The discovery or uncovering of the segmented Type 3 chip and its variants should be attributed to Shaw [64], while studying machining of Ti alloys (Shaw called it the "saw-tooth chip") and to Rice at Queens University in Canada [66]. In particular, the latter study and a companion paper [65], both surprisingly very little cited, characterized using high-speed cinematography and metallographic observations the key attributes of the segmented chip—the continuous segmented chip, as Rice labeled it. This labeling was done also to distinguish it from the discontinuous chip [72] often produced when cutting metals with very limited ductility (e.g., cast iron). In a sense, the Rice version is the truly segmented chip and is categorized as segmented Type 3 chip here; those highlighted by Shaw and Merchant are marked by shear bands and significant flow localization, and are (should be) classified as Type 4. Type 3 segmented chip has been observed even when cutting materials as diverse as extruded Al, 2-phase brass, steels, and even wax, justifying its importance as a fundamental chip type. The chip features highlighted—partially formed segments as in Fig. 4, occurrence of rupture or fracture to produce individual segments, periodicity of the segmentation (cyclic nature), and force oscillations in sync with the segmentation—pretty much encompass all the key attributes of this chip type as we know them today. However, key aspects of mechanics of this chip formation were not resolved in the Rice study, for example, how and where the rupture initiated, and its subsequent evolution; the resolution of the cinematography employed was not adequate for this purpose. These details were further elaborated upon in a subsequent high-speed photographic study of segmented chip formation in cold-rolled steel [57], wherein additional mesoscopic details of the segmentation process were presented. These pertained to shear plane oscillations during each segmentation event, occurrence of fracture possibly starting at the chip free surface, and crack formation facilitated by voids and second-phase particles. The machine-tool structure (e.g., stiffness) was also found to influence the segmentation. The conclusions, as regards key chip attributes, reinforced those of Rice [65].

The fundamental advance in understanding of segmented chip formation is due to the pioneering work of Nakayama on

"saw-tooth" chip formation [58], also a little-cited paper. In this paper, which mainly discusses results from observations of segmented chips, Nakayama presents a strong case for the segmentation being initiated by a crack occurring on the free surface of the chip, in the vicinity of the shear zone, this crack then propagating part-way toward the tool tip causing an individual segment to form. The recurring or cyclic occurrence of this cracking then leads to the segmented chip. Segmented chips were found to occur in various metals such as brass, Cu, Al, austenitic stainless steel, and Ti, when cutting with a tool of small rake angle (e.g., negative). Its occurrence was also promoted if the material was in an initially hardened state (e.g., pre-strained, heat treated). The cutting force in segmented chip formation was much lower than for Type 2 continuous chip, an observation that explained why cutting of hard metals was in several instances easier than cutting soft annealed metals. A simple analytical model [58] predicted that the surface crack triggering the segmentation was initiated at a critical value of the strain; this agreed with experimental results obtained from cutting of brass with tools of different rake angles. The Nakayama 1974 paper [58] is also remarkable for the breadth of its conclusions and topics—preference for segmented chips in cutting based on machinability considerations, contrary to prevailing views of that time (and even today) in favor of continuous Type 2 chips; difficulty in cutting of soft annealed metals; observations of a mechanochemical effect in cutting; and also, subsequently [75], for explaining some peculiarities in grinding of very hard steels (e.g., small forces) vis-à-vis soft steels (e.g., high forces), that could be traced directly back to segmented chip formation. Segmented chip formation was also found to be not restricted only to metals of low-workability but occurred in practically any metal if the tool rake angle is small (negative). Some of these results of Nakayama, especially about the propensity for segmentation at more negative rake angles were anticipated by Okushima and Hitomi [14]. They were perhaps also used in the first modeling of Type 3 chip formation by Obikawa and Usui [76] and Marusich and Ortiz [19], both of which incorporated fracture concepts—Usui, via introduction of a crack at the workpiece/chip free surface; and Marusich by incorporating a ductile failure (damage) criterion into the material model. Note that this type of incorporation of fracture/damage in FE modeling to simulate a segmented chip should be distinguished from suggestions such as by Atkins [77] to introduce fracture at the tool tip to simulate chip formation in general. Our group's work in the last 10 years has been strongly influenced by the Nakayama paper [58].

The segmented chip formation model of Nakayama received renewed attention in the 1990s with emerging interest in cutting of hard steels, wherein Type 3 chips are a common occurrence [56,78], but with signs of flow localization (shear bands?) in the regions between segments (Fig. 5). Shaw's work [56,78] re-emphasized the role of fracture in chip formation with hard steels, including also possible nucleation of cracks on the free surface of the chip and their propagation toward the tool tip. This was somewhat of an about-turn from his suggestion in the 1950s, following the discovery of segmented chip formation, that catastrophic/adiabatic shear (flow localization) is the reason for the segmentation [64]. A major reason for this change in outlook was the occurrence of this type of chip even in low-speed cutting, wherein flow localization is usually not observed. Strong evidence for the fracture-based model was provided by ex situ metallography of chips and tracking of markers on the workpiece surface, both of which revealed how various surfaces of the segmented chip formed [56,78]. The flow localization observed in Fig. 5 was attributed to the heat generated by relative sliding of the segments at high speeds (fracture propagation phase). An outgrowth of the observations was also a simple method for obtaining a measure of the chip strain from a "local" chip-thickness ratio, based on measurement of the step heights of the segments at the chip free surface. In contrast, other related works [79] postulated the flow localization to occur first, this localization then triggering the fracture; in this description of segmentation, the fracture location is left somewhat nebulous.

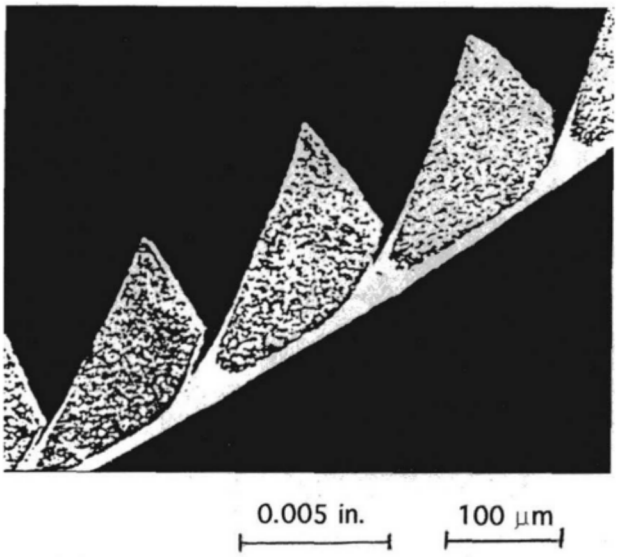

Fig. 5 Saw-tooth chip produced by cutting of hard carburized steel at 1.9 m/s. Adiabatic shear leads to the characteristic flow localization that gives rise to the saw-tooth appearance [78].

In our view, these "segmented chips" in hard steels, where strong flow localization is observed, should be classified as Type 4 shear-localized chips (seeSec. 5) and not as Type 3 segmented chips.

To illustrate various facets of segmented chip formation and its important attributes, we will utilize recent in situ observations of this chip formation based on high-speed image analysis and ex situ characterization and force measurements. Figure 6 shows four frames from a high-speed image sequence of cutting of hcp Zn (hardness = 37 HV) with $\alpha = -40$ deg tool, and at low-speed ($V_0 = 1$ mm/s) wherein temperature rise is negligible. The segmentation is triggered by a flow instability on the chip free surface, with the steps in the development of this instability being the following. A prow of material, inclined at angle θ to the workpiece surface, first develops ahead of the tool (frame 1) likely by shearing of surface elements along planes inclined at ~45 deg to the surface [81]. A crack then initiates on the prow surface (white arrow, frame 1), soon to be the chip free- (or back) surface and propagates toward the tool tip (frames 1 to 4, inter-frame time = 0.125 s) with a speed that is very similar to the cutting speed. This prow-crack formation represents the onset of the flow instability and constitutes the nucleation phase of segmentation. The (critical) prow angle θ^* when the crack forms is ~40 deg (frame 1). The flow is unsteady, as seen in the sequence. The motion of three points P_1, P_2, and P_3 (frame 2), tracked using PIV analysis, is used to describe the segmentation. P_1 and P_2 are initially very close to each other and on either side of an incipient crack tip. As the crack propagates toward the tool tip, the separation between P_1 and P_2 (frames 2–4) is increased up and until the crack is arrested. In Fig. 6, this arrest occurs approximately half-way between the chip free-surface and the tool tip (frame 4) due to a reduction in the crack-tip driving force. A new prow and crack now develop in a similar manner, and the process repeats cyclically. The relation between prow formation, crack nucleation, and the segmentation is obvious from Fig. 6. Segmented flow, with a similar development initiated by prow-cracking, has also been observed in cutting of 70–30 H02 brass [81], and even Cu and Al, the latter at larger (more) negative α. The observations largely confirm the Nakayama-Shaw model of the segmented chip formation.

In Zn, as well as in other alloys like brass, segmented flow driven by crack propagation from the chip free-surface occurs for a range of rake angles, from large negative α to zero, and sometimes even at somewhat positive α. In all instances, however, the distance of crack propagation towards the tool tip, that is segmentation

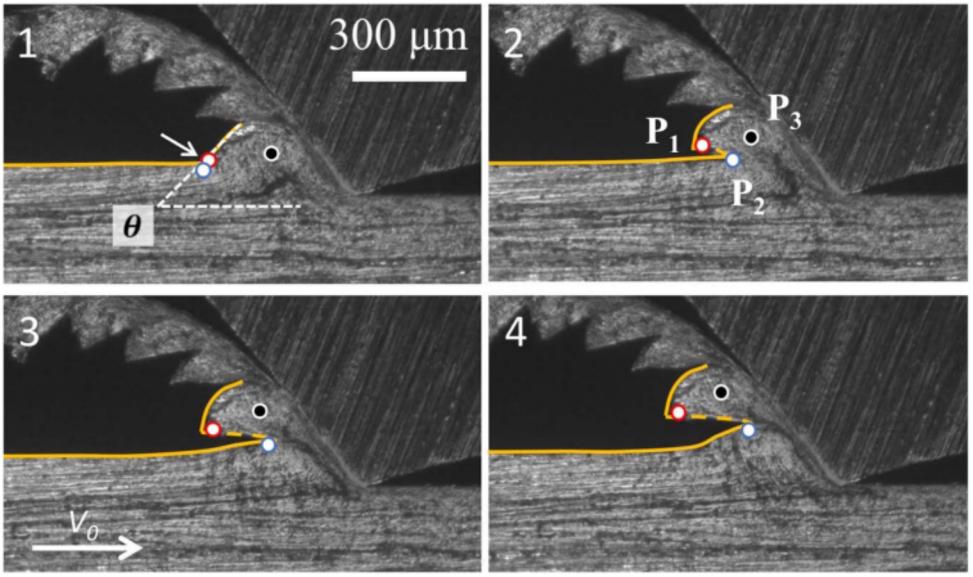

Fig. 6 Segmentation and flow dynamics in Zn cutting revealed by high-speed imaging [80]. $\alpha = 40$ deg, $V_0 = 1$ mm/s, $t_0 = 100\,\mu$m, inter-frame time = 0.125 s.

extent, is greater as α is decreased. Figure 7 shows this for two rake angles with the H02 70–30 brass. It is also clear from this figure that the roughness/waviness on the free surface of the chip due to the segmentation is geometrically similar, save for a scaling factor. This suggests that segmentation may be ubiquitous in cutting, occurring even at positive α but to a smaller extent; and it is this meso/micro-scale segmentation that manifests itself as the surface roughness usually seen on the free surface of even a Type 2 (continuous) chip. At the other extreme, in certain instances of cutting with large negative α, the crack propagates all the way to the tool tip resulting in a discrete chip particle—the (fully) discontinuous chip. Thus, segmentation appears to play a role both in the formation of discontinuous chips (large-scale segmentation) and Type 2 continuous chip with small-scale roughness; in the latter, the segmentation is confined to a very small region adjoining the chip free-surface.

The direct observations could capture the critical prow angle (θ^*) at crack initiation. Figure 8 shows the variation of θ^* with α for Zn and brass; this angle is remarkably constant (~37 deg, dotted line) for α between −60 deg and −10 deg—the parametric space corresponding to segmented flow. If prow formation is idealized as occurring by shearing of surface elements along planes inclined at 45 deg to the workpiece surface [80,81], then the prow angle θ is a direct measure of the surface strain in the prow; the shear strain is just 2θ (θ in radians), the corresponding von Mises effective strain (ε) is $2\theta/\sqrt{3}$, and $\varepsilon = 2\theta^*/\sqrt{3}$ is the surface strain at prow-crack initiation. That this is a good estimate of ε was also confirmed by direct PIV-based strain measurements from the high-speed image sequences [80,81]. The observed constancy in θ^* (Fig. 8) at failure therefore corresponds to a constancy in ε. Thus, the nucleation of segmentation appears to occur at a critical value of strain, this value being largely independent of deformation geometry (α), confirming Nakayama's predictions [58]. It may be noted here that such a critical strain (fracture) criterion is consistent with the simplest version of the Cockroft–Latham theory of ductile failure [82]. It would certainly be interesting to examine the dependence of this critical strain on material type. And the segmented chip formation geometry could provide a framework for exploring, more generally, ductile fracture in metals.

The above observations strongly suggest that the saw-tooth chips with flow localization observed in cutting of hardened steels [56,79] would fall in the category of Type 4 chips (see Sec. 5), per the classification of Nakayama used in this review, and not in Type 3 segmented category. It is very likely that in these instances, the flow

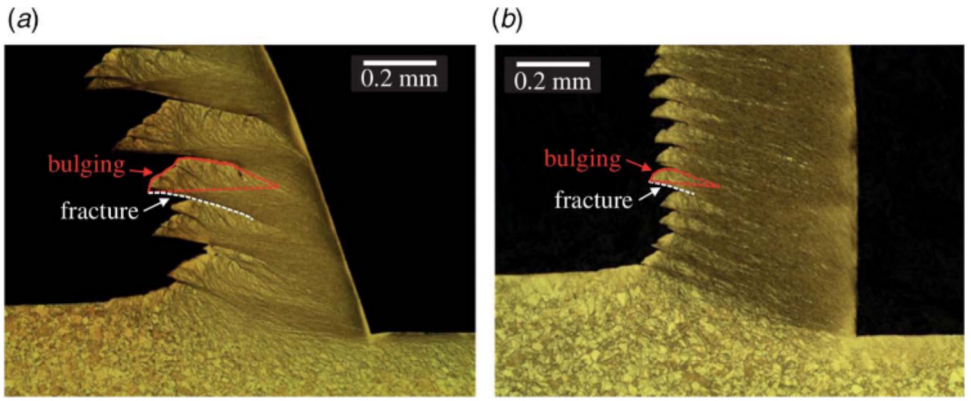

Fig. 7 Optical micrographs of etched "quick-stop" samples created by arresting the cutting in 70–30 brass [81]: (*a*) segmented Type 3 chip at $\alpha = -20$ deg and (*b*) continuous Type 2 chip at $\alpha = 0$ deg. The extent to which the crack runs into the chip increases as α is made more negative as indicated by the length of the white fracture lines.

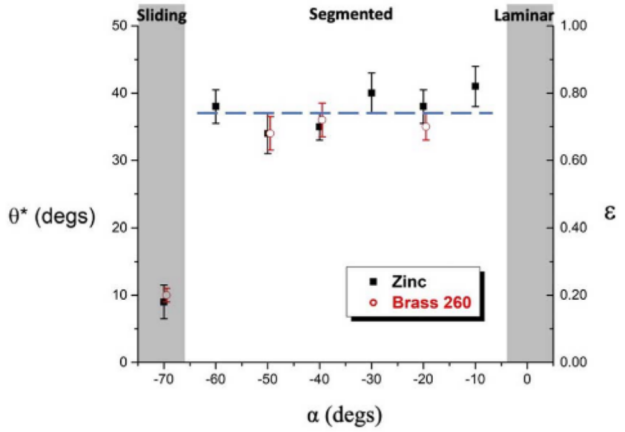

Fig. 8 Variation of prow angle at onset of cracking (θ^*) and prow strain (ε) with, α in cutting of Zn and 70–30 brass [80]. $V_0 = 1$ mm/s. The dotted line is a least square fit of the segmentation data.

localization in form of shear bands occurs first, beginning at the tool tip and spreading to the chip surface, followed by fracture.

The PIV analysis of flow also showed that the deformation in Type 3 chip is non-uniform, characterized by somewhat larger strain (~3X) in the fracture region between the segments compared to that within the segments. However, this flow heterogeneity is nowhere near as severe as in the case of the shear-localized Type 4 chip (see Sec. 5), thus providing another means to discriminate this chip from the morphologically similar Type 4. The last noteworthy observation pertains to segmentation morphology and forces. Figures 9(*a*) and 9(*b*) show the segment morphology across the chip width (back-surface, plan view) in the brass and Zn, respectively. While the segments run straight across the width in brass, they meander in Zn [80]. When observed from the side, however, both chips showed a similar saw-tooth appearance and were indistinguishable in terms of the morphology. This segmentation morphology difference was reflected in the forces (Fig. 9(*c*))—while force oscillations at the segmentation frequency were observed in the brass (straight segments), there was no discernible force oscillation in the Zn (meandering segments). Cutting experiments with other systems confirmed this to be a general phenomenon, that is, force oscillations occur only with the straight-segment morphology. In view of these observations, it should not be automatically assumed, as is commonly done, that segmentation is synonymous with force oscillations. The differences in segmentation morphology appear to have a microstructural origin, with ductility and grain size being the two principal factors in this regard. Similar morphology differences, also with a likely microstructure origin, have been observed with shear bands—CP–Ti (meandering) and Ti–6Al–4V (straight) [69].

5 Type 4 Chip and Shear-Flow Localization

The third important exception to laminar plastic flow in cutting is the cyclic chip formation that involves periodic localization of the flow to a few microns' thick layer, referred to as shear bands. This chip is also characterized by a saw-tooth morphology (Type 4, Fig. 4) and highly unsteady (non-laminar) plastic flow, which is best illustrated using SEM observations shown in Fig. 10. This chip shows very narrow bands of intense deformation, separated by large blocks or "segments" of relatively unstrained material (Fig. 10(*a*)). A zoomed-in view of one shear band is shown in Fig. 10(*b*), with the corresponding EBSD scan shown in Fig. 10(*c*). Concentration of intense shear to a ~5 μm thick layer (importantly, without fracture) is evident, although the internal

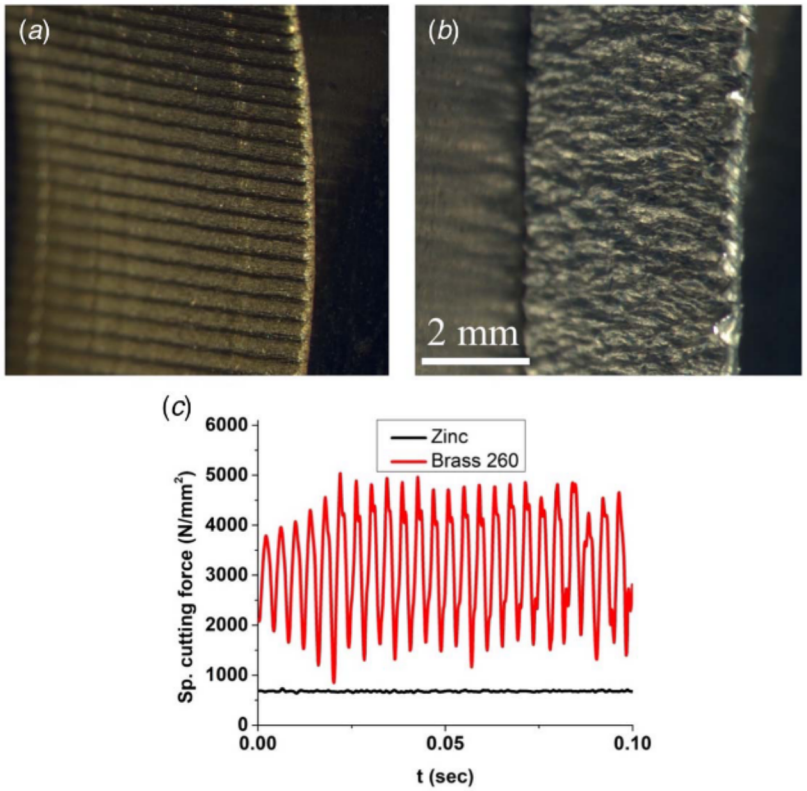

Fig. 9 Force oscillations (or lack thereof) in segmented chip formation reflect 3D chip morphology [80]. Optical micrograph of chip back-surface showing (*a*) straight segments in brass, $t_0 = 100$ μm, (*b*) meandering segments in Zn, $t_0 = 250$ μm, (*c*) specific cutting forces for (*a*) and (*b*) $\alpha = 5$ deg, $V_0 = 500$ mm/s.

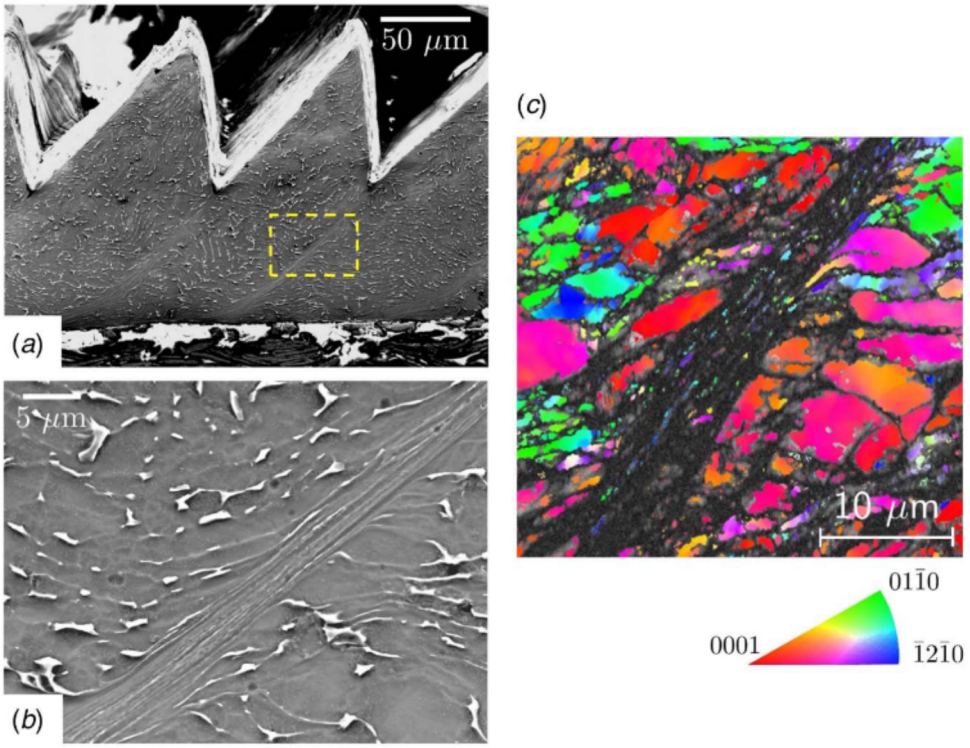

Fig. 10 Shear localization in machining [83]: (*a*) SEM image showing saw-tooth morphology of a shear-localized chip produced from Ti–6Al–4V at $V_0 = 5$ m/s. The image displayed in (*b*) is a magnified picture of the shear-localized region (shear band) within box in (*a*). (*c*) It shows EBSD inverse pole figure scan of regions surrounding the shear band. Intense localized flow within a thin shear band (<5 μm in thickness), without material separation or fracture, is evident.

microstructure of the band cannot be resolved in these images. Immediately adjoining the band are segments subjected to relatively small strains wherein the original workpiece grain structure is largely preserved. Since very large strains, typically exceeding 10 [69,84,85], are imposed in the shear band in a very short time (100 μs or less), the local strain rates and temperatures under which plastic flow occurs within the band are even more severe than in the case of laminar flow.

This highly localized flow mode in cutting has been referred to in the literature variously as catastrophic shear, adiabatic shear, shear banding, and serrated/saw-tooth chip formation [58,64,67,79,86–90]. We shall refer to this chip as the shear-localized chip (Type 4) in view of its most important visual attribute—intense deformation in a narrow band. Since the shear-localized chip is also sometimes confusingly called as a segmented chip, likely because of the similarity in the macroscopic chip appearance, it is important to distinguish between the respective underlying unsteady flow modes. As discussed earlier, in segmentation, the instability in the flow is triggered by nucleation and subsequent propagation of a ductile crack from the workpiece/chip surface region. On the other hand, as will be seen shortly, fracture is not a prerequisite for shear localization. Moreover, in segmentation, even though the deformation is inherently non-uniform, it is not highly localized as in the case of shear bands (~3X versus >10X). It is also important to distinguish shear localization at the mesoscale from other heterogeneous flow phenomena occurring at a microscopic or grain-level such as slip bands or shear front-lamellae [91–93]. That a shear band "cuts" across the material without apparent regard to the microstructure or grain boundaries is clear from Figs. 10(*b*) and 10(*c*).

The first observations of shear-localized chips in cutting appear to have been made by Shaw and Merchant [64,68], co-incidentally around the same time, during their studies on machining of Ti alloys. Subsequently, shear-localized chip formation was documented in other material systems such as hardened alloy steels, Ni-base superalloys, high-strength Al alloys and magnesium. The main factors that determine the occurrence of shear banding are the material's thermophysical properties and metallurgical state and cutting speed (V_0). In general, shear localization is favored by a combination of high strength, low thermal diffusivity, and high speed. Furthermore, in most metals, there is a "critical" transition speed only beyond which shear-localized chips are observed, with the flow mode being either laminar (Type 2) or segmented (Type 3) below this transition speed [67,79,86]. Certain exceptions to this general trend also exist, such as the popular Ti–6Al–4V alloy which exhibits shear localization over practically the entire range of speeds.

While observations of shear bands in highly deforming metals in themselves date back to at least 100–150 years, notably by Tresca [94,95], Massey and Russian researchers [96,97], it is Zener et al. [84,98] who should be credited with the first analysis of shear localization from a fundamental mechanics-materials standpoint. The landmark paper by Zener and Hollomon [98] is remarkable for its insight and casting of shear localization as a plastic flow instability problem arising from competing mechanisms involving material hardening (strain and strain rate hardening) and softening (deformation-induced temperature rise). Interestingly, the bulk of this paper is focused on the strain rate–temperature equivalence in metal plasticity, with only a few paragraphs at the end dedicated to flow localization. However, the most important idea from Zener's work is that at sufficiently high strain rates, when the heat generated due to plastic deformation has insufficient time for conduction, the deforming material becomes hot enough that its flow stress can decrease with strain; this is in contrast to the usual strain-hardening at quasi-static strain rates. The result of this effective "strain softening" is an instability wherein any small disturbance in the flow can lead to intense flow localization, since local increase in the plastic work of material leads to heat generation which further reduces the flow stress in its vicinity—an autocatalytic effect. Accordingly, for

a general flow stress function $\sigma = f(\varepsilon, \dot{\varepsilon}, T)$, the critical condition for the plastic flow to become unstable can be written as [99]

$$\frac{d\sigma}{d\varepsilon} = \left(\frac{\partial\sigma}{\partial\varepsilon}\right) + \left(\frac{\partial\sigma}{\partial\dot{\varepsilon}}\right)\cdot\left(\frac{\partial\dot{\varepsilon}}{\partial\varepsilon}\right) + \left(\frac{\partial\sigma}{\partial T}\right)\cdot\left(\frac{\partial T}{\partial\varepsilon}\right) = 0 \qquad (6)$$

where σ is the flow stress, ε is the effective plastic strain, $\dot{\varepsilon}$ is the plastic strain rate, and T is the temperature. Although originally proposed by Zener, this instability criterion appears to have been first formulated by Basinski, albeit in a slightly different form [100]. A good discussion of this formulation may be found in Backofen [99], from which in fact Eq. (6) is adapted. Note that, according to Eq. (6), it is the relative temperature rise and relative change in thermophysical/mechanical properties that determine the instability onset; the shear-banding type flow instability has been observed even at liquid He temperatures (~4 K) in uniaxial tensile deformation [101].

The application of the above (thermomechanical) instability criterion for machining appears to have been first done by Recht [67], and later extended by others [79,86,102]. Recht's five-page paper is noteworthy for its simplicity and utility in effectively capturing the flow transition from laminar to shear-localized type with increasing machining speed, and how the transition speed varies with the material's thermophysical properties. The work of Backofen [89,99,101] incorporated machine stiffness effects into the stability analysis and showed that a "soft" machine/system could further accelerate the onset of the flow instability; this brings to fore subtle but important contributions from the machine-tool structure and fixturing elements. Somewhat more recent developments in analytical modeling of shear localization include those based on nonlinear dynamics and perturbation type analyses [103,104]; these have attempted to capture also deformation-rate effects on shear band spacing and thickness. Other quantitative analysis of how shear localization develops in machining has come from FE simulations, where shear bands are triggered either by artificial introduction of a crack (at the tool tip or free surface) [19,76] or by appropriate choice of a constitutive material model with a flow-softening term [105–107]. Two recent FE studies [69,108] suggest that it may also be critically necessary to introduce some sort of damage accumulation into the material model, in order that the flow-softening necessary for the shear band instability can occur at the speeds observed in experiments.

Not surprisingly, phenomenological details of the shear-localization process such as band-initiation location, propagation dynamics, and force histories depend considerably on the model. Hence, it is generally not possible to discriminate between the various models, owing to lack of direct observations of shear localization in high-speed machining. Model validations currently are limited to comparison of simulation results with average cutting forces and post-mortem observations of chip morphology.

The experimental challenges associated with direct observation of shear bands come from their extremely small time and length scales. As an illustrative example, consider shear localization at V_0 of 1 m/s. If the spacing between shear bands is ~100 μm (a typical value), the frequency of shear band formation is ~10 kHz. This frequency is well beyond the natural frequency of common force dynamometers, which limits accurate characterization of cutting force oscillations. Furthermore, since the speeds at which localization occurs in most alloys are often >1 m/s, the above example provides only a conservative estimate of the band frequency. Similarly, if we assume that the shear offset distance on the free surface of the chip, formed as a result of localized "sliding" within the band, is of the same order of magnitude as band spacing (e.g., see Fig. 10(*a*)), and the shear band is inclined at about 45 deg with respect to V_0 direction, then it takes only ~50 μs for the entire process of shear localization (including nucleation and evolution) to be completed. Direct characterization of shear localization therefore calls for in situ imaging techniques such as high-speed photography. Furthermore, the typical shear band thickness of a few microns imposes additional requirements vis-à-vis spatial resolution. It is noteworthy that this need for in situ observations seems to have been recognized even in some of the earliest studies of the problem, see for example, the photography studies in Refs. [57,66,90], although these studies lacked the spatio-temporal resolution required for resolving the localized flow. Beginning with Ernst and Merchant, another important technique employed to understand the mechanism of shear localization is the so-called quick-stop method, wherein the tool and workpiece are quickly disengaged so as to interrupt the cutting, and the chip-root observed post-mortem. Based on quick-stop studies, the shear band instability (and localization) was described as propagating from the tool tip to the work/chip surface [15,87,109–111]. A diametrically opposite point of view, as discussed earlier and attributed to Shaw, is that the instability is triggered by crack formation at the free surface where workpiece meets the chip [56,58,112]. Note that quick-stop methods are not capable of resolving temporal details of shear band or crack initiation and can also introduce their own artefacts due to rapid unloading of the material. It may very well be that the aforementioned contradicting views on flow-instability development are rooted in some of these issues.

It is only with recent application of high-speed photography and high-resolution imaging, combined with marker techniques, that the different phases of shear-localized flow development are beginning to be uncovered, via in situ observations of the cutting process. Figure 11(*a*) is a high-speed image sequence showing different phases of the flow localization in cutting of Ti–6Al–4V (0.66 m/s). The localization occurs in two distinct phases, involving band initiation and sliding. The band initiation phase, where a well-defined "weak" plane OO′ is established, is quite fast (<25 μs), occurring between just two frames (*b* and *c*). The frames in the bottom row (*d*, *e*, and *f*) show the ensuing (second) sliding phase in which a whole chip segment/block "slips" along plane OO′ at a speed similar to the cutting velocity. While the initiation phase acts to "weaken" the material locally, intense localization of strain occurs predominantly during the sliding phase [69] as seen from the large material displacements in this phase. These large (sharp) displacements across the band (equivalent to strains >25) arising from local sliding can be seen in the SEM image of Fig. 11(*b*), wherein light markers are used to visualize the flow. One such marker, highlighted in yellow, illustrates the large shear offset (~100 μm) across the band. Our studies with highly cold-worked metals and low melting point metals, both of which exhibit the shear band instability at much lower speeds compared with Ti alloys and steels, have shown that the weak plane (OO′) actually forms via band nucleation at the tool tip and its subsequent propagation toward the free surface [69,70,113]. This is consistent with some of the ideas postulated using quick-stop studies [109,111]. The band propagation speed during the initiation phase is usually very much higher (~10 times > V_0) than the speed at which the sliding occurs in the second phase. The latter velocity V_S is found to be simply the component of V_0 resolved along the shear band plane, i.e., $V_S \approx \cos(\alpha)\cdot V_0/\cos(\phi)$, where ϕ is the included (shear) angle between the band and V_0.

Unlike in case of mode II (shear) fracture, the sliding at the shear band plane and attendant strain localization occur while maintaining physical material continuity across the band. That the displacements across the band result purely from highly localized shear, and not from fracture, is clearly seen from the continuity of the markers (equivalently streaklines) across the band (Fig. 11(*b*)). As for the cracks that are sometimes observed on the free surface of a shear-localized chip (e.g., see Fig. 5) [58,78,112], the in situ imaging studies suggest that they are formed during the sliding phase, that is well after the band nucleation, and therefore cannot be the cause for the flow instability [70]. A question does arise, however, regarding how material within the shear-localized zone can sustain such large strains, sometimes exceeding 50! [69].

From a processing standpoint, shear localization is generally to be avoided since high-frequency force oscillations due to periodic band formation can have adverse implications for surface finish and tool life. This may be seen from Fig. 12 where a shear-localized

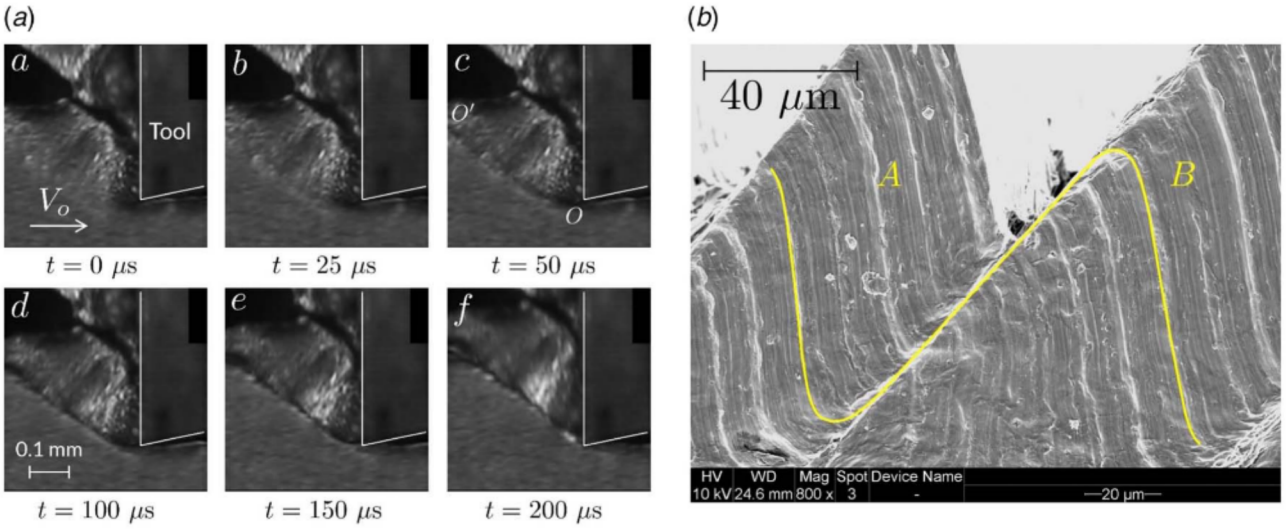

Fig. 11 (*a*) High-speed image sequence (40,000 frames per second) showing different phases involved in the development of shear localization in Ti–6Al–4V ($V = 0.66$ m/s) [69]. Frames (*a*)–(*c*) show initiation of a "weak" plane OO′, followed by sliding along this plane in frames (*d*)–(*f*). Intense localized strains are developed during this unconstrained sliding phase. (*b*) SEM image of shear-localized Ti–6Al–4V chip showing profile of micromarkers (light striations on the chip) across the shear band separating two neighboring segments (*a*) and (*b*). One marker is highlighted to illustrate large displacements across the band. The markers were initially scribed onto the workpiece surface.

chip (generated using quick-stop method) and the corresponding machined surface produced in austenitic stainless steel are shown. Periodic localization of plastic flow in the chip, albeit to a lesser degree than in Ti–6Al–4V, is visible in Fig. 12(*a*). More importantly, the machined surface produced under this localization condition has undulations, besides significant microstructure inhomogeneity; for example, see at arrow in Fig. 12(*b*), which marks the location on the machined surface that has been subjected to a higher strain compared to adjoining regions. This figure also reinforces the notion that deformation history and microstructure of the machined workpiece surface "mirrors" that of the chip. Hence the equivalence between chip and surface deformation, well-established for continuous Type 2 chip formation (laminar flow) [32], may also be a characteristic of chip formation (types) where flow instabilities/localization occur. In some instances, flow localization may be desirable, for it can be exploited to carry out material deformation (e.g., punching, cutting) with reduced forces/energy [80,84]. However, it is only very recently that this aspect is beginning to receive attention in the context of cutting [80].

In view of the aforementioned, sometimes adverse and other times beneficial, consequences of flow localization, a capability to control localization, or any other unsteady flow (e.g., segmentation) for that matter, is of vital interest in processing. By control is meant here, both suppression and enhancement of the unsteady flow and the instability triggering it. A promising approach for suppressing shear localization in machining is by inhibiting the sliding phase, wherein much of the localization strain (>90%) develops, through application of a macroscopic constraint to the chip formation [22,23,69,80]. This constraint, in the form of a second die, is placed directly across from the cutting tool edge, thereby fixing the exit (deformed) chip thickness t_c; the chip formation becomes now akin to a metal forming process [21,80]. Figure 13 demonstrates this band suppression in a magnesium alloy. Conventional machining results in the formation of discrete chip particles (Fig. 13(*a*)) due to severe shear banding and subsequent fracture; whereas with the application of the constraint, the discrete chips are now replaced by a long continuous ribbon chip (Fig. 13(*b*)). That the flow localization in the chip is also fully suppressed can

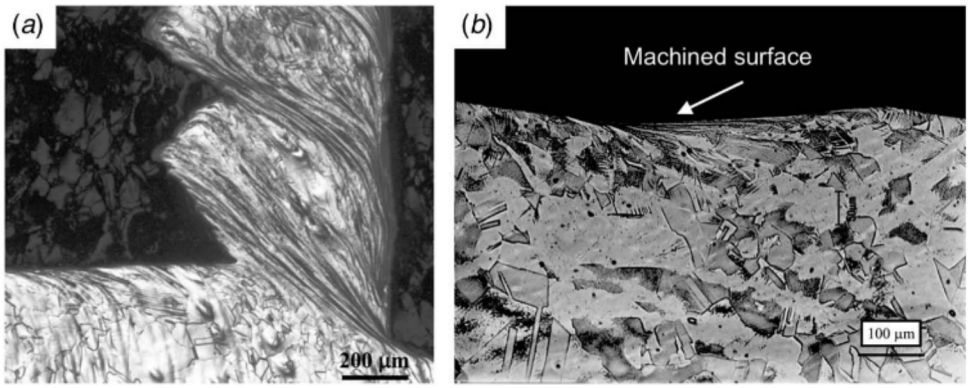

Fig. 12 Correlation between flow localization in chip and workpiece surface features: (*a*) typical shear-localized chip produced in austenitic stainless steel at $V_0 \sim 2$ m/s and $t_0 = 300\ \mu$m. The corresponding machined surface is shown in (*b*). This surface is seen to have an undulating morphology. Deformation heterogeneity on the machined surface can be also inferred from the non-uniform microstructure (see at arrow).

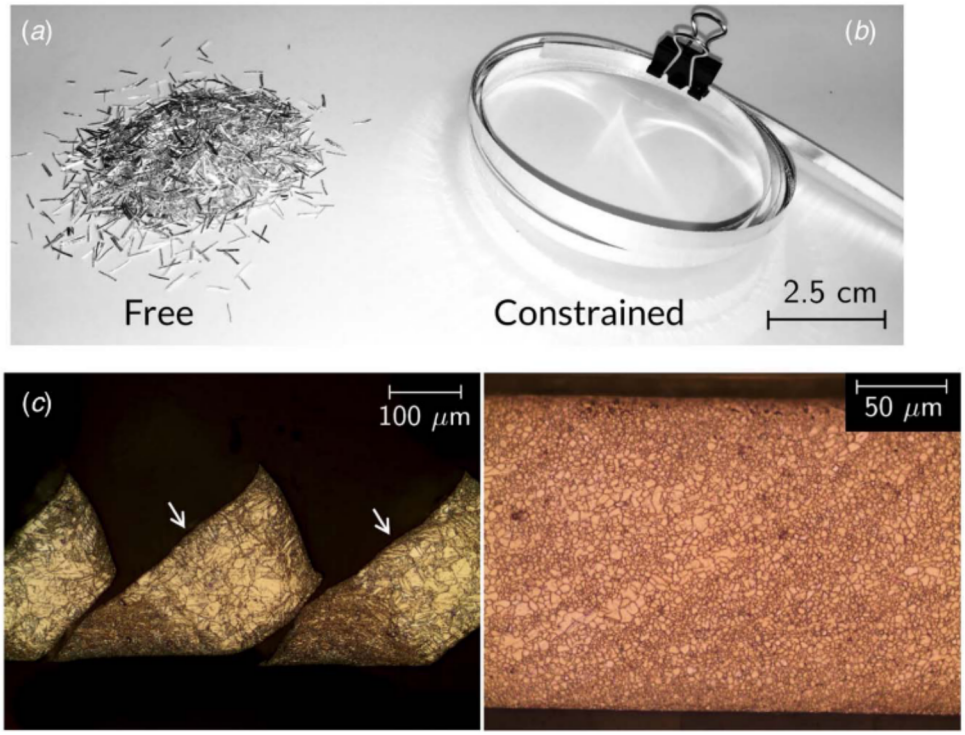

Fig. 13 Suppression of unsteady flow by application of geometric constraint in cutting [69]: (*a*) and (*b*) show the transition from discrete chip formation in conventional cutting (without constraint) to continuous strip with the application of geometric constraint across the tool ($t_c/t_0 = 0.7$) in Mg alloy AZ31B. This transition is due to suppression of the shear band sliding phase. (*c*) Optical micrographs of the etched chip cross-sections. The highly non-uniform deformation (shear localization) in discrete chips from free-machining may be noted, while the continuous strip produced by constrained chip formation is characterized by a homogeneous and fully dynamically recrystallized microstructure.

be seen from the optical micrograph of Fig. 13(*c*). This approach which is purely geometric has also been found to be effective in suppressing shear bands in Ti and Ni-base alloys, as well as segmentation flow [80]. The potential benefits of controlling unsteady shear band and segmentation flows for improving machined surface integrity or process attributes such as forces, stability, and tool life remain to be explored.

6 Type 1 Chip and Sinuous Flow

The final exception to smooth laminar flow is Type 1 chip formation (Fig. 4(*a*)) [58]. This chip, very thick with irregular mushroom-shaped structures and "cracks" on its free surface, is commonly observed when cutting "gummy" metals—a common machine-shop term [61]. To date, metal-machining literature has focused largely on cutting of metal alloys of moderate-to-high strength. This work has shown, among other things, the poor machinability of alloys such as hardened steels and Ti to arise from their high hardness and propensity for shear banding and segmentation. Based on these observations, one may be led to assume that a soft metal (low hardness) is easy to machine. While this is true in cases like lead and tin (negligible strain-hardening), paradoxically, the vast majority of soft metals (e.g., Cu, Al, Ta, Fe, and Nb) and some of their alloys are actually very difficult to machine and grind, characterized by large forces (Fig. 14(*a*)), thick chips, inhomogeneous deformation, and excessive side flow. In drilling deep holes, for example, the forces are often high enough to fracture the drill. More generally, this difficult-to-machine characteristic is symptomatic of metal alloys that have a high strain-hardening capacity, including Ni alloys, stainless steels, and low-carbon steels (the soft pure metals also fall in this highly strain-hardening category). Thus, the gummy metals may be said to be composed of the class of highly strain-hardening metals.

The earliest recognition of the difficulty in cutting soft metals was probably by Mallock [114], who described the formation of a thick chip with a helpful illustration akin to Fig. 4(*a*). This difficulty was attributed to high friction between chip and tool. A systematic study on the cutting of pure metals such as annealed Cu, Al, and Fe by Williams et al. [59] and Trent [41] established their poor machinability, including occurrence and morphology of the thick Type 1 chip (Fig. 14(*b*)). The chip formation was analyzed using the shear plane model [59], with very small shear-angles, <10 deg estimated (as will be seen, the underlying flow in these metals is at variance with the shear plane model). The mushroom-shaped features on the chip back-surface were postulated to arise from surface cracks. Furthermore, machinability was found to improve significantly, viz. thinner chips, smaller forces, when the metals were cut in an initially work-hardened condition. Nakayama's paper on saw-tooth chip formation [58] made very insightful observations concerning the difficulty of cutting soft metals, especially its close connection with the occurrence of Type 1 chip. Furthermore, these observations could also explain the unusually large tangential force (power component) seen in grinding of soft (150 HV) mild steel [75], which was ~50% greater than that in grinding of 700 HV hardened steel (Fig. 14(*c*)). The mild steel chips were thicker (Type 1, $\lambda \sim 3$) than those from the hardened steel (Type 3, $\lambda \sim 1$) indicating much more straining in the former case. Additional problems in the machining of soft and/or highly strain-hardening metals are poor surface finish [41], and tangled coils of continuous chips that are difficult to evacuate from the machining zone. In drilling, tapping, and analogous cutting processes with these metals, the tangled chips clog the flutes or spaces between the cutter teeth, limiting productivity and contributing to tool fracture.

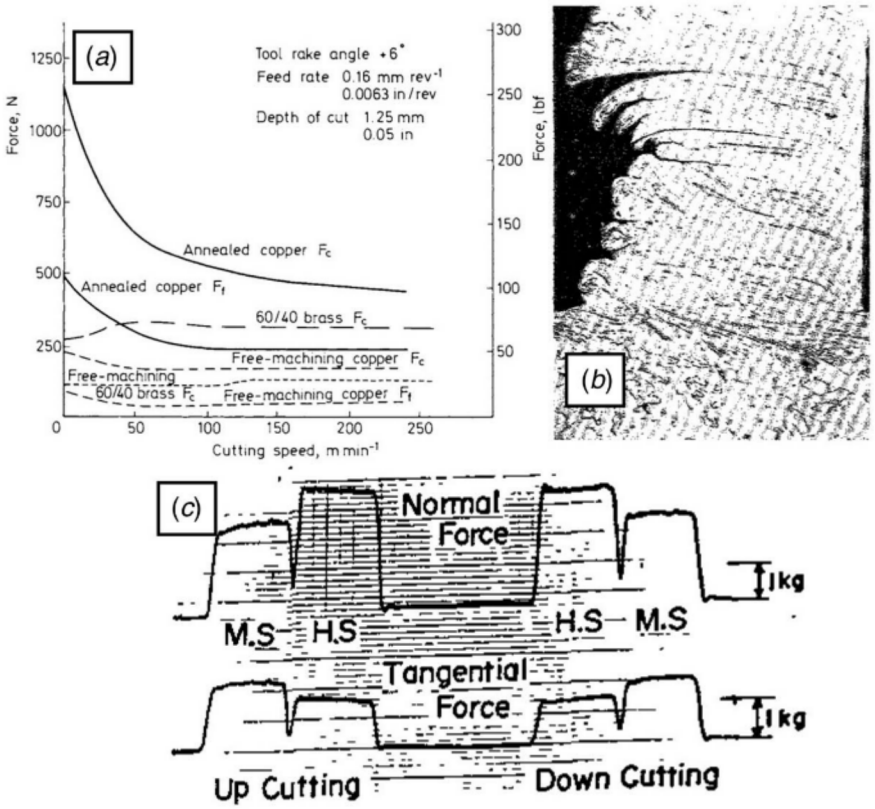

Fig. 14 Early observations of difficulties in machining soft metals: (*a*) Cutting annealed copper requires significantly higher forces than cold-worked copper [41], (*b*) the chip that forms when cutting soft metals (pure iron) is very thick and has mushroom-shaped features on the free-surface [59], and (*c*) grinding mild steel requires higher tangential force than hardened steel [75] (Reprinted with permission from Elsevier © 1974).

To better understand why soft metals and highly strain-hardening metals are difficult to cut, and its connection with Type 1 chip formation, we carried out studies using high-speed in situ imaging [60,62]. By digitally processing the images, it is possible to obtain a comprehensive record of material flow, strain, and strain rate histories. Figure 15(*a*) shows the flow of material in the deformation zone, highlighted using streaklines, and the formation of a very thick chip ($t_c/t_0 \sim 14$) when cutting annealed OFHC Cu (~60 HV). The flow is characterized by highly sinewy streaklines and large-amplitude material folding; the peak-to-peak amplitude in a single fold often being as much as two-thirds of the chip thickness. The chip is thus composed of a series of folds stacked up on top of each other. It is these folds that appear as the mushroom-shaped structures characteristic of Type 1 chip, with the regions between the folds (creases) giving the appearance of cracks. It is clear from Fig. 15(*a*) that there is significant redundant deformation associated with this flow. The folding and redundant deformation give rise to a non-homogenous strain field in the chip, see the

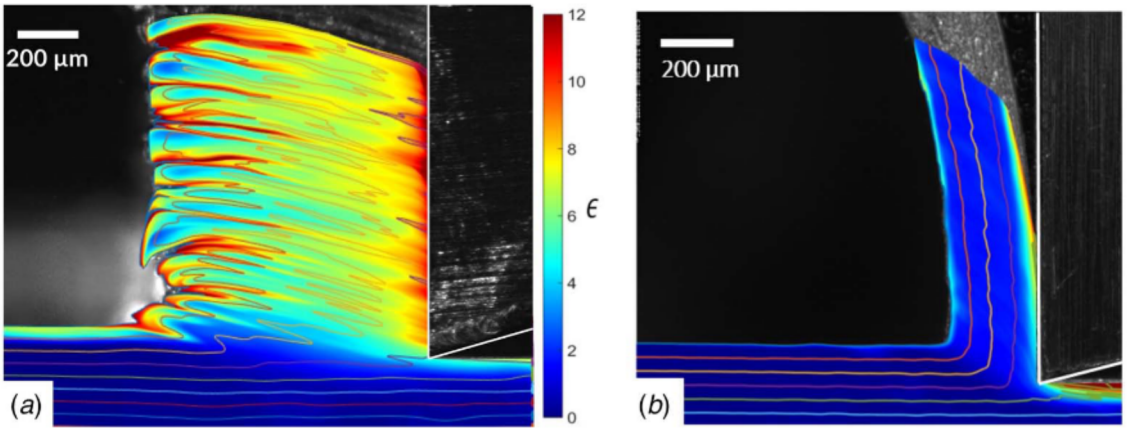

Fig. 15 Comparison of material flow, deformation and chip morphology when cutting annealed and hardened Cu. Background color map shows the strain field. [115] (*a*) Sinuous flow produces a thick chip ($t_c/t_0 = 14$) in annealed Cu. The strain field is heterogeneous (non-uniform), and the average strain is ~7. (*b*) Laminar flow produces thin chip ($t_c/t_0 = 2$) in cold-worked Cu. The strain field is homogeneous with uniform strain ~3.

background color map in Fig. 15(*a*); this field is characterized by large plastic strains of 4–8. However, the degree of non-homogeneity (variation) in strain is no more than a factor of 3 which is much less severe than in shear-band flow. Because of its wavy appearance, this type of flow has been called sinuous flow [60]. Based on examination of the streakline pattern, folding, and the strain field, it is clear that this sinuous flow does not develop via a shear plane mechanism. Sinuous flow represents a new mesoscale, unsteady plastic flow mode in the same genre as the laminar, shear band, and segmented flows already discussed.

When the same OFHC Cu is cut in an initially pre-strained (hardened, 160 HV) condition (~2), the chip forms via laminar flow and is of Type 2 see Figs. 15(*b*) and 1(*b*). The laminar flow field is characterized by smooth streaklines and a uniform strain (Fig. 15(*b*)). This flow arises from a well-defined and confined deformation zone that very much resembles a shear plane, as evident from the strain rate field of Fig. 1(*b*). The contrast between sinuous flow (Fig. 15(*a*)) and laminar flow associated with a stable shear plane (Figs. 1(*b*) and 15(*b*)) is quite striking.

The principal stages in sinuous flow development can be seen in Fig. 16, which shows select frames from a high-speed image sequence. The flow is nucleated by the formation of a bump ahead of the tool/chip (frame A), that is very suggestive of a plastic (column) buckling process occurring at the workpiece surface [116,117]. The bump or buckle as it forms is "pinned" between two material points P1 and P2, these points constituting the column extremities. As the tool advances, the buckle grows in height while decreasing in width (frames B and C), thus evolving into a fold [63,118]. The fold is then rotated and sheared as the material slides up the tool face (frame D). The entire buckling then repeats, leading to a series of folds that stack up on top of each other to form the chip. The sinuous flow with folding represents a stable, albeit unsteady, mesoscale plastic flow mode.

Based on these observations, the relation between the mushroom-shaped features on the chip back-surface and folds should now be clear. There is no cracking occurring visible on the chip back-surface, as has been previously suggested. It is only the fold-interfaces that appear as cracks. The folding also explains how the very thick chip develops without resorting to a model that invokes a small shear plane angle and high tool friction. It is very unlikely that the formation of Type 1 chip, by folding and sinuous flow, could have been inferred purely from post-mortem observations, illustrating also the power of in situ imaging in uncovering flow features.

Figure 17(*a*) shows the forces in cutting of the annealed and pre-strained (hardened) Cu [62]. The cutting force for annealed Cu is very large, three times as high as for the work-hardened Cu, even though the latter material is ~2.5 times as hard as the former. The higher forces (energy) in the annealed Cu are due to the formation of the very thick Type 1 chip, with large strains, folding and redundant deformation. Despite the repeated folding events, the sinuous flow force does not show any oscillations. This is because the sinuous flow deformation is not perfectly two-dimensional; that is, each fold does not run straight across the entire width of the chip but meanders due to the grain structure (see Fig. 17(*b*)), similar to the segmented flow in Zn (Fig. 9(*b*)). Consequently, multiple asynchronous folding events occur through the width of the chip, that average out any force oscillations. The very thick Type 1 chip with underlying sinuous flow is thus the cause for the "gumminess," and all its undesirable consequences, in cutting of soft and/or highly strain-hardening metals; and not laminar flow with a very small-angle shear plane.

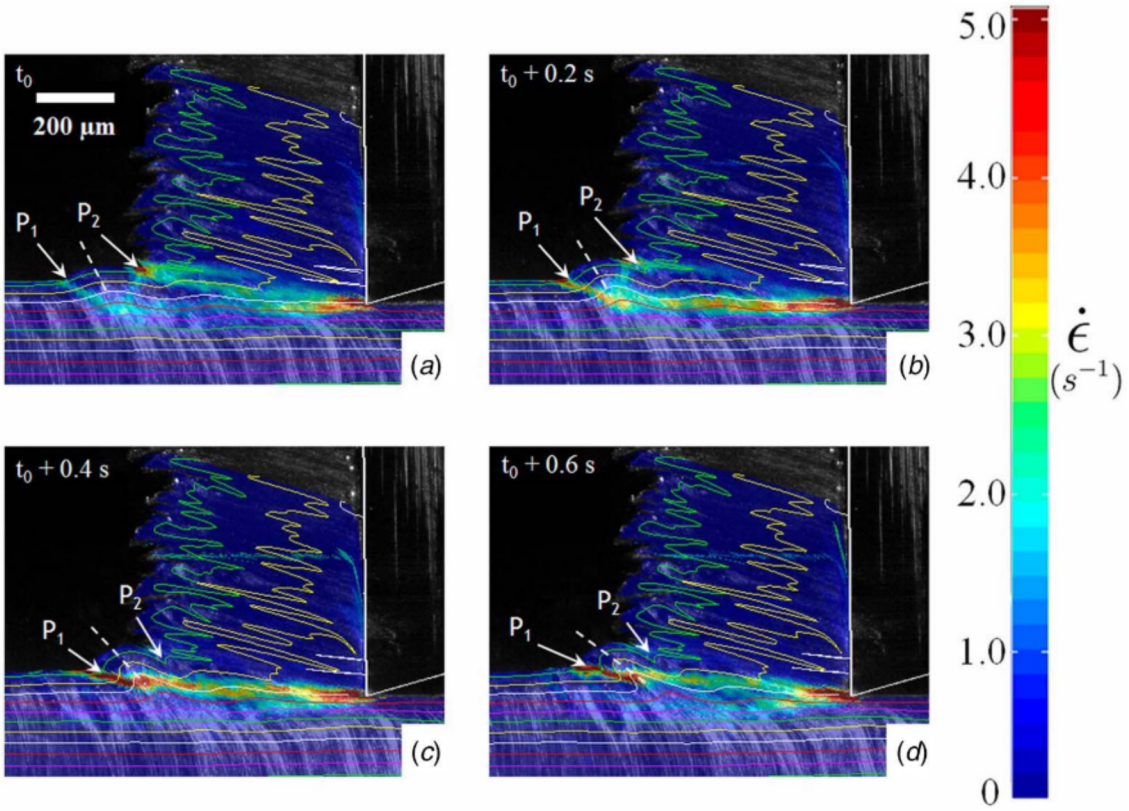

Fig. 16 Sequence of images with superimposed streaklines showing buckling, folding and development of sinuous flow in cutting of annealed Cu [60]. The underlying strain rate field (background color) captures regions of local deformation. (*a*) P1 and P2 (marked by white arrows) are material locations that delimit the initial bump. These provide the pinning points for the surface buckle in (*b*). Upon further advance of the tool (*c*), this bulge rotates and is stretched diagonally, before finally forming an incipient fold between points P1 and P2 in (*d*).

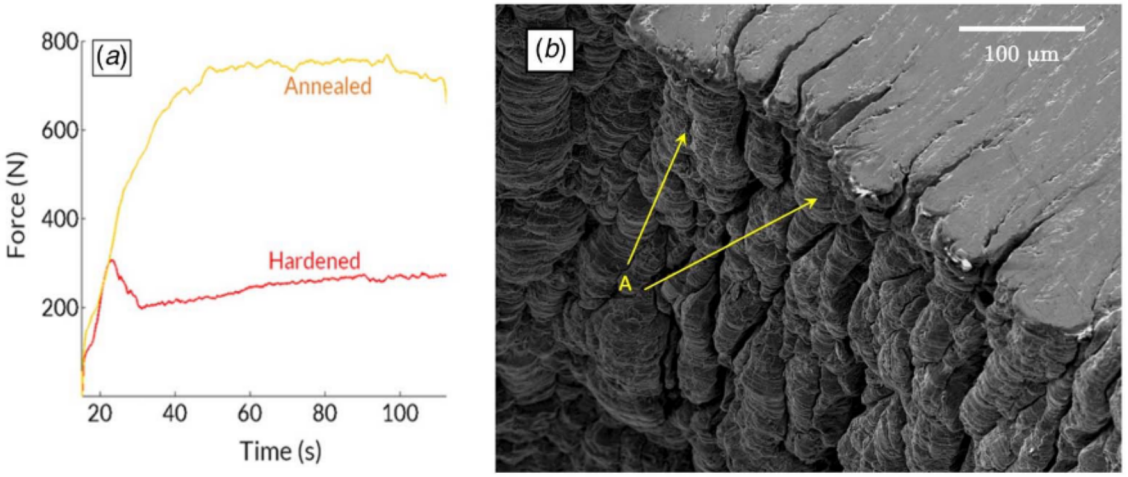

Fig. 17 Cutting forces and Type 1 chip morphology [62]. (*a*) The force due to sinuous flow (annealed Cu, Type 1 chip) is much larger (3X) than in cutting of hardened Cu (Type 2 chip) where laminar flow prevails [62]. (*b*) SEM image of Type 1 chip (back or free) surface showing folds (see at arrows) that meander across the chip width.

How can these difficulties in machining of gummy metals be mitigated to improve machinability? One approach is to cut these metals with a highly positive rake-angle tool; under such conditions, laminar flow with Type 2 chip and significantly lower forces are observed to prevail. A more recent, and intriguing, solution is by use of surface-active media that adsorb onto the initial workpiece surface [119,120]. Such media were found to cause a local ductile-to-brittle transition in the deformation zone, with the flow switching from sinuous to segmented and a Type 3 chip resulting with significantly smaller forces. Media that have been found to be effective in producing this switchover include common metal-marking inks and glues, and even Sharpie!

7 Summary

We can now summarize the principal points pertaining to mechanics of large-strain deformation in cutting of metals.

(1) Chip formation occurs by shear deformation under conditions of extreme strain and high strain rate that is confined to a small region—the shear plane or shear zone. The deformation conditions of strain and strain rate, and strain path, are determined by the deformation geometry, namely rake angle and chip-thickness ratio, and by the speed. Chip formation, hence, can also be viewed as a controlled large-strain deformation process or SPD process, this being even more the case in constrained cutting wherein the exit thickness of the chip is fixed a priori.

(2) The large-strain deformation and strain path result in extraordinary refinement of the workpiece microstructure as it transforms into the chip, often into the sub-micron, even sub-100 nm range. To first-order, this microstructure is also inherited by the workpiece surface. The unique deformation conditions in chip formation, and their controllability, open up possibilities for utilizing machining as a method for studying SPD microstructures; and assessing high strain rate properties of metal alloys.

(3) The plastic flow processes at the mesoscale determine the chip morphology or type—in fact, there is a one-to-one correlation between the underlying flow and chip morphology. The principal chip types are the continuous chip produced by smooth laminar flow (Type 2); the segmented chip characterized by a fracture instability (Type 3); the shear-localized chip formed by severe flow localization within narrow micron-sized regions (Type 4); and the very thick Type 1 chip, characterized by sinuous flow and folding, that typically forms when cutting highly strain-hardening metals. Flow instabilities play a key, over-arching, role in the formation of these chips and their morphology. Except for Type 2 chip, the other chip types (morphologies) are all a consequence of highly, unsteady plastic flow triggered by flow instabilities—shear bands, buckling and fracture. This suggests opportunities also for using the machining framework to obtain fundamental insights into plastic instability phenomena in large-strain deformation.

(4) Process attributes such as forces and energy, and chip/workpiece attributes such as microstructure and mechanical properties are a direct consequence of the underlying plastic flow phenomena.

We conclude the review with a discussion, albeit somewhat speculative, of how plastic flow phenomena control the emergence of the various chip types; and a framework wherein these chip types, and, by extension, the process and workpiece properties can be predicted.

8 Stability Considerations, Plasticity, and the Nature of the Chip

Given the different chip morphologies involved in metal cutting, it is natural to ask if there are basic overarching principles that govern their formation. It should be clear by now that chip formation is quite intimately tied to the underlying plastic flow process, as seen from the four principal chip types discussed. The plastic flow process, especially near free surfaces as in machining, depends on the workpiece material and process conditions. But can we place these considerations in a framework that has predictive capabilities, while also enabling improved conceptual/phenomenological understanding?

To address this question, it is instructive to revisit Merchant's original model and the minimum energy criterion for the shear plane angle [7,9]. (As highlighted earlier, but worth reiterating, the deformation geometry in cutting (ϕ), unlike bulk forming processes, is not fixed a priori, but is an outcome of the underlying flow process.) Since ϕ is a priori unknown, this criterion, or at least some variant, at first seems necessary for picking a unique value of ϕ [121]. However, it is difficult to rationalize the minimum energy criterion from first principles for large-strain plastic flow, unlike for quasi-static elastic deformation where

reversibility and lack of dissipation ensure that the actual deformed state is one of minimum strain energy.

The question of whether the shear plane angle, and consequently, the chip deformation geometry is unique has since been much debated. Hill [122] analyzed the possibility that the shear plane might not be unique after all and that, for a given material–process parameter combination, a range of ϕ could be allowed. To follow Hill's analysis, consider the standard (steady) chip configuration shown in Fig. 1(*a*) with rake α, shear plane ϕ, and friction angle β ($= \tan^{-1}\mu$, with μ the tool–chip friction coefficient). By applying limits on stress singularities allowed [123] in the plastically deforming chip (assumed rigid-perfectly plastic), it may be shown that ϕ should lie within a broad "permissible range" determined by β and α; with all of the associated deformation fields obeying the equilibrium equations. This non-uniqueness of ϕ, in Hill's own words, reflects the fact that "there may be many, even infinitely many, steady-state configurations of a given type." Similar analyses, along with additional plastic field solutions, have also been provided subsequently by Kudo [124], Roth [125], and Dewhurst [126].

However, as experimental results for the laminar flow (Type 2) chip show, this is hardly the case. For given conditions of workpiece pre-strain and deformation geometry, the shear plane orientation appears to be nominally fixed and robust to external perturbation (e.g., vibrations). Therefore, the possibility of several allowed ϕ solutions to the plasticity equations has little bearing on the actual ϕ observed, which in reality is likely decided by some physical (likely extremum) principle. The constraining assumption of rigid plastic material behavior, a simplification used in these analyses, could be the reason for the incorrect ϕ predictions (i.e., non-unique ϕ).

This possibility is bolstered by the in situ experimental observations discussed earlier. For instance, when cutting highly strain-hardening materials, energies measured for the very thick Type 1 chip, involving unsteady sinuous flow with extensive redundant deformation, are lower than for a corresponding hypothetical Type 2 chip (laminar flow) with the same chip-thickness ratio [60]. Even though this latter (hypothetical) configuration is deemed permissible by the aforementioned analyses, it does not occur in reality. The logical conclusion is that smooth laminar flow itself is suspect in many situations (Types 1, 3, and 4). Therefore, before we even try to predict ϕ accurately, it is important to predict the operative plastic flow mode, and consequently the chip type, while cutting a certain metal with a particular deformation geometry.

This brings us back to the basic question of how the very thick Type 1 chip forms. Given the wealth of information about plastic flow in chip formation revealed by the in situ imaging and other microscopic techniques, we can now address this query in a more general framework. As explained earlier, Type 1 chip development is intimately tied in with the repeated formation of bumps on the workpiece surface ahead of the chip. Recent experimental evidence has revealed that this surface bump formation occurs by a plastic buckling instability. To elucidate, consider an elastic column under uniaxial compression. Up until the load P reaches a critical value P_c—the Euler buckling load—the deformation is homogeneous; beyond this load, the column buckles. The analogous plastic case is conceptually identical, involving plastic instead of elastic buckling [116,117], so that at a critical load, an alternate deformation path becomes more viable. The same physical process occurs during formation of a Type 1 chip, with the alternate path to laminar flow being initiated by plastic buckling, followed by folding [60,62]. Here, it may be analytically shown that the buckling route in fact requires lower force than that for the corresponding laminar flow [63]. This repeated surface plastic buckling is the underlying cause for the unsteady mode of plastic flow—sinuous flow—and resulting Type 1 chip.

Just as with plastic buckling, one could envisage other instabilities triggering unsteady flows in lieu of laminar flow. These provide alternative deformation pathways leading to different chip types. For instance, at a critical plastic strain, crack nucleation can becomes favorable on the chip free surface [58,80,81], providing a path for the segmented Type 3 chip. Here, laminar flow is disrupted by an alternate deformation path via crack nucleation and growth, the latter constituting the flow instability. With Type 4 chip, a shear localization instability periodically disrupts laminar flow [64,67,69]. This localization could be of adiabatic origin [67] or involve more detailed considerations of strain and damage accumulation [69,99,102].

The different (alternate) deformation pathways can be cast into a common "phase diagram" that indicates the regimes wherein a particular type of chip might occur, see Fig. 18 [120]. The default plastic deformation mode in this figure is one of uniform deformation and laminar flow. The vertical axis represents a material property (initial workpiece state (pre-strain)) and the horizontal axis, a key process property, viz., deformation geometry (rake angle). One could equally well envisage a situation with additional material/process axes. The lower curve that demarcates occurrence of plastic buckling is shown in red and that for crack nucleation is shown on top in blue (there will be similar curves, not yet incorporated, for shear banding and/or other instabilities that may be uncovered). For a given experiment, the initial material state and process condition used define a point in the figure, say point A. If the experimental conditions were such that no instabilities were favorable, then laminar flow would ensue, and the shear plane/zone mode would be applicable. Then the shear plane orientation is seen to fall in a narrow zone, determined by the initial conditions. However, the morphology of Type 2 chip is, qualitatively, the same in each case. If the experimental conditions were such that points B or C represented the initial state, then chip formation would occur not by laminar flow, but instead by the corresponding instability at B (buckling) or C (crack nucleation). In either case, an alternative deformation pathway is favored, so that Type 1 or Type 3 chip should form instead.

It is clear from this phase diagram that the earlier notions of "a whole range of steady-state solutions of say the shear plane type, each complete in a technical sense and each associated with a set (or sets) of initial conditions by an intervening non-steady transitional flow" [122] which, admittedly somewhat vague, can now be quantified and made precise. This picture of flow stability critically influencing (controlling) the chip formation process is a recent

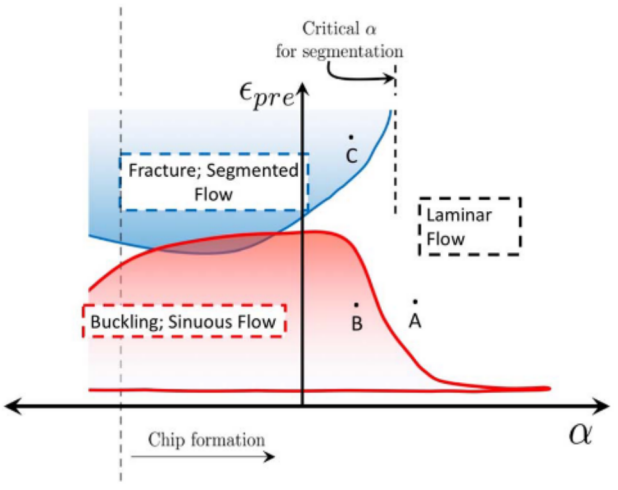

Fig. 18 Phase diagram showing stability domains of different plastic-flow modes [120]. Any point in the diagram corresponds to a single experiment specified by the deformation geometry (α) and initial deformation state (pre-strain, ϵ_{pre}) of workpiece surface. A point by default is assumed to be in the laminar flow regime (point A). If it is under the lower (red) curve, then laminar flow will give way to sinuous flow (point B); if over the top (blue) curve, then laminar flow will give way to periodic segmentation (point C).

idea [120]—our proposal—that we believe warrants significant quantitative investigation.

9 Concluding Remarks and Suggestions for the Future

The mechanics of large-strain deformation in cutting of metals is reviewed, with an emphasis on recent developments in analyses of plastic flow, using in situ imaging, and microstructure; complemented by highlights from classical work. The large-strain deformation field is shown to be controllable via the input process parameters. A strong connection is established between plastic deformation/flow modes that prevail in the deformation zone and four principal types (morphologies) of chip formation, with each of the four chip types and associated process attributes shown to arise from a distinct flow mode. Plastic flow instabilities such as shear banding, buckling, and fracture, are seen to play a critical role in mediating the flow modes. These flow phenomena determine process/workpiece attributes such as forces, energy, deformation, and microstructure. A proposal is made, synthesizing various observations into a phase diagram, that it is the stability of plastic flow modes that determines the mechanics of the cutting process; this suggests a predictive framework for machining processes.

The key role played by plastic flow phenomena, especially flow stability, in determining the chip formation and, hence, process outcomes, suggests some avenues and unresolved questions for exploration.

(1) Examine and validate the hypothesis that plastic flow stability is the principal factor determining chip formation. Formalize the establishment of metal-cutting phase diagrams, analogous to Fig. 18, in the "right" process/material framework. This will require both in situ and ex situ characterization of the cutting in an appropriate experimental setting (experimental design), complemented by modeling.
(2) How does microstructure influence large-strain plastic flow phenomena, including flow instabilities? How does the flow mode (chip type) affect surface integrity?
(3) How does one incorporate microstructure, flow stability, and damage accumulation in modeling/simulation? One must envisage doing this in some sort of semi-continuum framework so that the simulations are sufficiently large-scale (and multi-scale) to make ensemble-level predictions of deformation/process parameters and material outcomes (e.g., microstructure, properties).
(4) Utilize detailed deformation measurements such as derived from in situ imaging and marker techniques, and microstructure/properties characterization, to further the validation of metal cutting models/simulations.
(5) Expand machining-based methods for materials manufacturing; and as test methods for studying materials behavior, including constitutive properties, under extreme deformation conditions. This is a consequence of the connection between controllability of deformation field parameters and microstructure/texture in machining, briefly highlighted in the review in the context of using machining as a method of SPD.

Acknowledgment

SC would like to thank the students and post-doctoral fellows at Purdue (1987–present) who have contributed in no small measure to the work appearing in this review. We, the authors as a group, have also greatly benefited from discussions with many colleagues and researchers in the manufacturing and materials communities. Various aspects of the Purdue work discussed in this review have been supported over the years by the NSF, ARO, and DOE, and companies including Cummins, Timken, General Motors, Saint Gobain, Ford, M4 Sciences, and Seco Tools. We also thank Elsevier, Royal Society (UK), Cambridge University Press, and the American Physical Society for giving us permission to reproduce various figures. The preparation of this paper was supported in part by DOE EERE Award DE-EE000786 and NSF Grants CMMI 1562470 and DMR 1610094 to Purdue and SERB Grant CRG/2018/002058 (Government of India) to KV.

Dedication

This review is dedicated to Professor Milton C Shaw—a pioneer, among other things, in highlighting the role of large-strain plasticity in metal cutting, the subject matter of this review; and who has influenced so many of us with his wide-ranging contributions in manufacturing and tribology. Milton Shaw, who passed away on September 7, 2006, at the age of 91, was exemplary as an engineer/scientist; an outstanding mentor of students and post-doctoral researchers; and an individual of warmth, generosity, tenacity, and modest habits. Shaw made extraordinary contributions to manufacturing, materials processing, and tribology, over a research career spanning 60 years. In his own words, he changed his field approximately every 10 years, beginning with tribology and trailblazing through metal cutting, large strain deformation, abrasive processes, design, and fracture. Interestingly, like Merchant, with whom he shared a doctoral fellowship, his entry into metal cutting was via tribology. He was elected to the U.S. National Academy of Engineering in 1968 for his contributions to chemical synthesis, lubrication and bearing design, and machine tool design and performance. He very much emphasized the conceptual approach to problem solving, emphasizing engineering solutions that could be effectively used by practitioners. His academic scholarship inspired and will continue to inspire generations of engineers and engineering educators. We would like to refer readers to the website[2] that documents his life and research contributions.

References

[1] Mullins, W. W., and Shaw, M. C., 1968," Metal Transformations: Informal Proceedings of the Second Buhl International Conference on Materials, Pittsburgh, PA, Gordon and Breach.
[2] Ernst, H., and Merchant, M. E., 1941, "Chip Formation, Friction and Finish, Surface Treatment of Metals," ASM Symposium: The Surface Treatment of Metals, pp. 299–378.
[3] Ernst, H., 1938, "Physics of Metal Cutting," ASM Symposium on Machining of Metals, American Society of Metals, Cleveland, OH, pp. 1–34.
[4] Shaw, M. C., 1954, *Metal Cutting Principles*, M.I.T. Press, Cambridge, MA.
[5] Shaw, M. C., 1950, "A Quantized Theory of Strain Hardening as Applied to the Cutting of Metals," J. Appl. Phys., **21**(6), pp. 599–606.
[6] Shaw, M. C., 1944, "Action of N-Primary Alcohols as Metal Cutting Fluids—Alternating Properties with Chain Length," J. Am. Chem. Soc., **66**(12), pp. 2057–2059.
[7] Merchant, M. E., 1945, "Mechanics of the Metal Cutting Process. I. Orthogonal Cutting and a Type 2 Chip," J. Appl. Phys., **16**(5), pp. 267–275.
[8] Merchant, M. E., 1945, "Mechanics of the Metal Cutting Process. II. Plasticity Conditions in Orthogonal Cutting," J. Appl. Phys., **16**(6), pp. 318–324.
[9] Piispanen, V., 1937, "Lastun Muodostuminen Teoria," Tek. Aikakausl. (in Finnish), **27**, p. 315. See translation at Piispanen, V., 1948, "Theory of Formation of Metal Chips," J. Appl. Phys., **19**(10), p. 876–881.
[10] Lee, E. H., and Shaffer, B. W., 1951, "The Theory of Plasticity Applied to Machining," ASME J. Appl. Mech., **18**(4), pp. 405–413.
[11] Oxley, P. L. B., 1989, *Mechanics of Machining: An Analytical Approach to Assessing Machinability*, Ellis Horwood, West Sussex, England.
[12] Kobayashi, S., and Thomsen, E. G., 1962, "Metal-Cutting Analysis Re-Evaluation and New Method of Presentation of Theories," ASME J. Eng. Ind., **84**(1), pp. 63–70.
[13] Palmer, W. B., and Oxley, P. L. B., 1959, "Mechanics of Orthogonal Machining," Proc. Inst. Mech. Eng., **173**(1), pp. 623–654.
[14] Okushima, K., and Hitomi, K., 1961, "An Analysis of the Mechanism of Orthogonal Cutting and Its Application to Discontinuous Chip Formation," ASME J. Eng. Ind., **83**(4), pp. 545–555.
[15] Ramalingam, S., 1967, "Plastic Deformation in Metal Cutting," Ph.D. thesis, University of Illinois.
[16] Strenkowski, J. S., and Carroll, J. T., 1985, "A Finite Element Model of Orthogonal Metal Cutting," ASME J. Eng. Ind., **107**(4), pp. 349–354.
[17] Shih, A. J., 1995, "Finite Element Simulation of Orthogonal Metal Cutting," ASME J. Eng. Ind., **117**(1), pp. 84–93.

[2] https://sites.google.com/umich.edu/shihlabs/prof-milton-shaw/the-life-of-professor-milton-shaw

[18] Usui, E., and Shirakashi, T., 1982, "Mechanics of Machining—From Description to Predictive Theory," *On the Art of Cutting Metals- 75 Years Later*, ASME, New York, pp. 13–35.
[19] Marusich, T. D., and Ortiz, M., 1995, "Modelling and Simulation of High-Speed Machining," Int. J. Numer. Methods Eng., **38**(21), pp. 3675–3694.
[20] Madhavan, V., Chandrasekar, S., and Farris, T. N., 2000, "Machining as a Wedge Indentation," ASME J. Appl. Mech., **67**(1), pp. 128–139.
[21] De Chiffre, L., 1990, "Metal Cutting: Mechanics and Applications," Ph.D. thesis, Technical University of Denmark.
[22] Efe, M., Moscoso, W., Trumble, K. P., Dale Compton, W., and Chandrasekar, S., 2012, "Mechanics of Large Strain Extrusion Machining and Application to Deformation Processing of Magnesium Alloys," Acta Mater., **60**(5), pp. 2031–2042.
[23] Moscoso, W., Shankar, M. R., Mann, J. B., Compton, W. D., and Chandrasekar, S., 2007, "Bulk Nanostructured Materials by Large Strain Extrusion Machining," J. Mater. Res., **22**(1), pp. 201–205.
[24] Ramalingam, S., and Black, J. T., 1972, "On the Metal Physical Considerations in the Machining of Metals," ASME J. Eng. Ind., **94**(4), pp. 1215–1224.
[25] Zorev, N. N., 1966, *Metal Cutting Mechanics*, Pergamon Press, Oxford, England.
[26] Kececioglu, D., 1958, "Shear-Strain Rate in Metal Cutting and Its Effects on Shear-Flow Stress," Trans. ASME, **80**(1), p. 158.
[27] Kececioglu, D., 1960, "Shear-Zone Size, Compressive Stress, and Shear Strain in Metal-Cutting and Their Effects on Mean Shear-Flow Stress," ASME J. Eng. Ind., **82**(1), pp. 79–86.
[28] Brown, T. L., Swaminathan, S., Chandrasekar, S., Compton, W. D., King, A. H., and Trumble, K. P., 2002, "Low-Cost Manufacturing Process for Nanostructured Metals and Alloys," J. Mater. Res., **17**(10), pp. 2484–2488.
[29] Childs, T. H. C., 1971, "A New Visio-Plasticity Technique and a Study of Curly Chip Formation," Int. J. Mech. Sci., **13**(4), pp. 373-387.
[30] Lee, S., Hwang, J., Shankar, M. R., Chandrasekar, S., and Dale Compton, W., 2006, "Large Strain Deformation Field in Machining," Metall. Mater. Trans. A, **37**(5), pp. 1633–1643.
[31] Gnanamanickam, E. P., Lee, S., Sullivan, J. P., and Chandrasekar, S., 2009, "Direct Measurement of Large-Strain Deformation Fields by Particle Tracking," Meas. Sci. Technol., **20**(9), p. 095710.
[32] Guo, Y., Saldana, C., Dale Compton, W., and Chandrasekar, S., 2011, "Controlling Deformation and Microstructure on Machined Surfaces," Acta Mater., **59**(11), pp. 4538–4547.
[33] Brown, T. L., Saldana, C., Murthy, T. G., Mann, J. B., Guo, Y., Allard, L. F., King, A. H., Compton, W. D., Trumble, K. P., and Chandrasekar, S., 2009, "A Study of the Interactive Effects of Strain, Strain Rate and Temperature in Severe Plastic Deformation of Copper," Acta Mater., **57**(18), pp. 5491–5500.
[34] Swaminathan, S., Ravi Shankar, M., Rao, B. C., Compton, W. D., Chandrasekar, S., King, A. H., and Trumble, K. P., 2007, "Severe Plastic Deformation (SPD) and Nanostructured Materials by Machining," J. Mater. Sci., **42**(5), pp. 1529–1541.
[35] Swaminathan, S., Shankar, M. R., Lee, S., Hwang, J., King, A. H., Kezar, R. F., Rao, B. C., Brown, T. L., Chandrasekar, S., Compton, W. D., and Trumble, K. P., 2005, "Large Strain Deformation and Ultra-Fine Grained Materials by Machining," Mater. Sci. Eng. A, **410–411**, pp. 358–363.
[36] Shankar, M. R., Rao, B. C., Lee, S., Chandrasekar, S., King, A. H., and Compton, W. D., 2006, "Severe Plastic Deformation (SPD) of Titanium at Near-Ambient Temperature," Acta Mater., **54**(14), pp. 3691–3700.
[37] Saldana, C., Swaminathan, S., Brown, T. L., Moscoso, W., Mann, J. B., Compton, W. D., and Chandrasekar, S., 2010, "Unusual Applications of Machining: Controlled Nanostructuring of Materials and Surfaces," ASME J. Manuf. Sci. Eng., **132**(3), p. 030908.
[38] Pu, Z., Yang, S., Song, G.-L., Dillon, O. W., Puleo, D. A., and Jawahir, I. S., 2011, "Ultrafine-Grained Surface Layer on Mg–Al–Zn Alloy Produced by Cryogenic Burnishing for Enhanced Corrosion Resistance," Scr. Mater., **65**(6), pp. 520–523.
[39] Embury, J. D., and Fisher, R. M., 1966, "The Structure and Properties of Drawn Pearlite," Acta Metall., **14**(2), pp. 147–159.
[40] Langford, G., and Cohen, M., 1969, "Strain Hardening of Iron by Severe Plastic Deformation," ASM Trans. Quart., **62**(3), pp. 623–638.
[41] Trent, E. M., 1977, *Metal Cutting*, Butterworths, London.
[42] Jackson, P. S., and Wright, P. K., 1982, "Application of Plastic Boundary Layer Theory to Metal Machining," ASME J. Eng. Ind., **104**(4), pp. 358–362.
[43] Wright, P. K., Horne, J. G., and Tabor, D., 1979, "Boundary Conditions at the Chip-Tool Interface in Machining: Comparisons Between Seizure and Sliding Friction," Wear, **54**(2), pp. 371–390.
[44] Dautzenberg, J. H., and Zaat, J. H., 1973, "Quantitative Determination of Deformation by Sliding Wear," Wear, **23**(1), pp. 9–19.
[45] Drucker, D. C., 1949, "An Analysis of the Mechanics of Metal Cutting," J. Appl. Phys., **20**(11), pp. 1013–1021.
[46] Thomsen, E. G., and Lapsley, J. T., Jr., 1954, "Experimental Stress Determination Within a Metal During Plastic Flow," Proc. Soc. Exp. Stress Anal., **11**(2), pp. 59–68.
[47] Attia, M. H., and Kops, L., eds., 1988, "Thermal Aspects in Manufacturing," ASME-PED.
[48] Saldana, C., Murthy, T. G., Shankar, M. R., Stach, E. A., and Chandrasekar, S., 2009, "Stabilizing Nanostructured Materials by Coherent Nanotwins and Their Grain Boundary Triple Junction Drag," Appl. Phys. Lett., **94**(2), p. 021910.
[49] Lu, K., Lu, L., and Suresh, S., 2009, "Strengthening Materials by Engineering Coherent Internal Boundaries at the Nanoscale," Science, **324**(5925), pp. 349–352.
[50] Wang, Y., Chen, M., Zhou, F., and Ma, E., 2002, "High Tensile Ductility in a Nanostructured Metal," Nature, **419**(6910), pp. 912–915.
[51] Dalla Torre, F., Lapovok, R., Sandlin, J., Thomson, P. F., Davies, C. H. J., and Pereloma, E. V., 2004, "Microstructures and Properties of Copper Processed by Equal Channel Angular Extrusion for 1-16 Passes," Acta Mater., **52**(16), pp. 4819–4832.
[52] Valiev, R. Z., and Langdon, T. G., 2006, "Principles of Equal-Channel Angular Pressing as a Processing Tool for Grain Refinement," Prog. Mater. Sci., **51**(7), pp. 881–981.
[53] Steeds, J., 1966, "Dislocation Arrangement in Copper Single Crystals as a Function of Strain," Proc. R. Soc. A, **292**(1430), pp. 343–373.
[54] Kobayashi, A., 1967, *Machining of Plastics*, McGraw-Hill, New York.
[55] Armarego, E. J. A., and Brown, R. H., 1969, *The Machining of Metals*, Prentice-Hall, Englewood Cliffs, NJ.
[56] Shaw, M. C., and Vyas, A., 1993, "Chip Formation in the Machining of Hardened Steel," CIRP Ann., **42**(1), pp. 29–33.
[57] Komanduri, R., and Brown, R. H., 1980, "On the Mechanics of Chip Segmentation in Machining," ASME J. Eng. Ind., **103**(1), pp. 33–51.
[58] Nakayama, K., 1974, "The Formation of 'Saw-Toothed Chip' in Metal Cutting," Proceedings of International Conference on Production Engineering, Tokyo, pp. 572–577.
[59] Williams, J. E., Smart, E. F., and Milner, D. R., 1970, "The Metallurgy of Machining. Part I: Basic Considerations and the Cutting of Pure Metals," Metallurgia, **81**(483), pp. 3–10.
[60] Yeung, H., Viswanathan, K., Compton, W. D., and Chandrasekar, S., 2015, "Sinuous Flow in Metals," Proc. Natl. Acad. Sci. U. S. A., **112**(32), pp. 9828–9832.
[61] Schneider, G., 2009, "Machinability of Metals," Am. Mach.
[62] Yeung, H., Viswanathan, K., Udupa, A., Mahato, A., and Chandrasekar, S., 2017, "Sinuous Flow in Cutting of Metals," Phys. Rev. Appl., **8**(5), p. 054044.
[63] Udupa, A., Viswanathan, K., Ho, Y., and Chandrasekar, S., 2017, "The Cutting of Metals via Plastic Buckling," Proc. R. Soc. A, **473**(2202), p. 20160863.
[64] Shaw, M. C., Dirke, S. O., Smith, P. A., Cook, N. H., Loewen, E. G., and Yang, C. T., 1954, "Machining Titanium," MIT Report to U. S. Air Force.
[65] Rice, W. B., 1961, "The Formation of Continuous Chips in Metal Cutting," Can. Eng. J., pp. 41–45.
[66] Salmon, R., Rice, W. B., and Russel, L. T., 1962, "Force Variation During the Formation of Continuous Segmented Chips in Metal Cutting," Can. Eng. J., pp. 59–62.
[67] Recht, R. F., 1964, "Catastrophic Thermoplastic Shear," ASME J. Appl. Mech., **31**(2), pp. 189–193.
[68] Merchant, M. E., Krabacher, E. J., Young, H. W., and Miller, J. H., 1954, "Titanium Is Unorthodox When Machined… Here's Why," Am. Mach., **98**, p. 118.
[69] Sagapuram, D., Viswanathan, K., Mahato, A., Sundaram, N. K., M'Saoubi, R., Trumble, K. P., and Chandrasekar, S., 2016, "Geometric Flow Control of Shear Bands by Suppression of Viscous Sliding," Proc. R. Soc. A, **472**(2192), p. 20160167.
[70] Yadav, S., Feng, G., and Sagapuram, D., 2019, "Dynamics of Shear Band Instabilities in Cutting of Metals," CIRP Ann., **68**(1), pp. 45–48.
[71] Cook, N. H., Finnie, I., and Shaw, M. C., 1954, "Discontinuous Chip Formation," Trans. ASME, **76**(2), pp. 153–162.
[72] Field, M., and Merchant, M. E., 1949, "The Mechanics of the Formation of the Discontinuous Chip in Metal Cutting," Trans. ASME, **71**, p. 421.
[73] Gane, N., 1979, "Fracture During the Machining of Brass," Fracture at Work: Fourth Tewksbury Symposium, D. S. Mansell, and G. H. Vasey, eds., Melbourne, pp. 13.1–13.22.
[74] Enahoro, H. E., and Oxley, P. L. B., 1961, "An Investigation of the Transition From a Continuous to a Discontinuous Chip in Orthogonal Machining," Int. J. Mech. Sci., **3**(3), pp. 145–156.
[75] Nakayama, K., Takagi, J., and Nakano, T., 1974, "Peculiarity in the Grinding of Hardened Steel," CIRP Ann., **23**(1), pp. 89–90.
[76] Obikawa, T., and Usui, E., 1996, "Computational Machining of Titanium Alloy —Finite Element Modeling and a Few Results," ASME J. Manuf. Sci. Eng., **118**(2), pp. 208–215.
[77] Atkins, A. G., 2003, "Modelling Metal Cutting Using Modern Ductile Fracture Mechanics: Quantitative Explanations for Some Longstanding Problems," Int. J. Mech. Sci., **45**(2), pp. 373–396.
[78] Vyas, A., and Shaw, M. C., 1999, "Mechanics of Saw-Tooth Chip Formation in Metal Cutting," ASME J. Manuf. Sci. Eng., **121**(2), pp. 163–172.
[79] Davies, M. A., Burns, T. J., and Evans, C. J., 1997, "On the Dynamics of Chip Formation in Machining Hard Metals," CIRP Ann., **46**(1), pp. 25–30.
[80] Saei, M., Udupa, A., Viswanathan, K., Sugihara, T., M'Saoubi, R., and Chandrasekar, S., 2019, "Controlling Segmentation in Cutting of Metals," CIRP Ann., **68**(1), pp. 41–44.
[81] Guo, Y., Compton, W. D., and Chandrasekar, S., 2015, "In Situ Analysis of Flow Dynamics and Deformation Fields in Cutting and Sliding of Metals," Proc. R. Soc. A, **471**(2178), p. 20150194.
[82] Cockcroft, M. G., and Latham, D. J., 1968, "Ductility and the Workability of Metals," J. Inst. Met., **96**(1), pp. 33–39.
[83] Sagapuram, D., and Viswanathan, K., 2018, "Evidence for Bingham Plastic Boundary Layers in Shear Banding of Metals," Extreme Mech. Lett., **25**, pp. 27–36.
[84] Zener, C., 1948, "The Micro-Mechanism of Fracture," *Fracturing of Metals*, American Society of Metals, Cleveland, OH, pp. 3–31.

[85] Marchand, A., and Duffy, J., 1988, "An Experimental Study of the Formation Process of Adiabatic Shear Bands in a Structural Steel," J. Mech. Phys. Solids, **36**(3), pp. 251–283.
[86] Komanduri, R., and Hou, Z. B., 2002, "On Thermoplastic Shear Instability in the Machining of a Titanium Alloy (Ti-6Al-4V)," Metall. Mater. Trans. A, **33**(9), pp. 2995–3010.
[87] Komanduri, R., and von Turkovich, B. F., 1981, "New Observations on the Mechanism of Chip Formation When Machining Titanium Alloys," Wear, **69**(2), pp. 179–188.
[88] Childs, T., 2014, "Adiabatic Shearing in Metal Machining," *CIRP Encyclopedia of Production Engineering*, Springer, Berlin, Heidelberg, pp. 27–33.
[89] Lemaire, J. C., and Backofen, W. A., 1972, "Adiabatic Instability in the Orthogonal Cutting of Steel," Metall. Mater. Trans. B, **3**(2), pp. 481–485.
[90] Komanduri, R., 1993, "Machining and Grinding: A Historical Review of the Classical Papers," ASME Appl. Mech. Rev., **46**(3), pp. 80–132.
[91] Ramalingam, S., and Black, J. T., 1973, "An Electron Microscopy Study of Chip Formation," Metall. Trans., **4**(4), pp. 1103–1112.
[92] Black, J. T., 1972, "Shear Front-Lamella Structure in Large Strain Plastic Deformation Processes," ASME J. Eng. Ind., **94**(1), pp. 307–313.
[93] von Turkovich, B. F., 1970, "Shear Stress in Metal Cutting," ASME J. Eng. Ind., **92**(1), pp. 151–157.
[94] Johnson, W., 1987, "Henri Tresca as the Originator of Adiabatic Heat Lines," Int. J. Mech. Sci., **29**(5), pp. 301–310.
[95] Dodd, B., and Bai, Y., 2012, *Adiabatic Shear Localization*, Elsevier, New York.
[96] Kravz-Tarnavskii, V. P., 1928, "A Peculiar Band Discovered in Steel (in Russian)," J. Russ. Metall. Soc., **3**, pp. 162–167.
[97] Dodd, B., Walley, S. M., Yang, R., and Nesterenko, V. F., 2015, "Major Steps in the Discovery of Adiabatic Shear Bands," Metall. Mater. Trans. A, **46**(10), pp. 4454–4458.
[98] Zener, C., and Hollomon, J. H., 1944, "Effect of Strain Rate upon Plastic Flow of Steel," J. Appl. Phys., **15**(1), pp. 22–32.
[99] Backofen, W. A., 1972, *Deformation Processing*, Addison-Wesley, Reading, MA.
[100] Basinski, Z., 1957, "The Instability of Plastic Flow of Metals at Very Low Temperatures," Proc. R. Soc. A, **240**(1221), pp. 229–242.
[101] Chin, G. Y., Hosford, W. F., and Backofen, W. A., 1964, "Influence of the Mechanical Loading System on Low-Temperature Plastic Instability," Trans. Metall. Soc. AIME, **230**(5), pp. 1043–1049.
[102] Semiatin, S. L., and Rao, S. B., 1983, "Shear Localization During Metal Cutting," Mater. Sci. Eng., **61**(2), pp. 185–192.
[103] Burns, T. J., and Davies, M. A., 1997, "Nonlinear Dynamics Model for Chip Segmentation in Machining," Phys. Rev. Lett., **79**(3), pp. 447–450.
[104] Molinari, A., Musquar, C., and Sutter, G., 2002, "Adiabatic Shear Banding in High Speed Machining of Ti-6Al-4V: Experiments and Modeling," Int. J. Plast., **18**(4), pp. 443–459.
[105] Hua, J., and Shivpuri, R., 2004, "Prediction of Chip Morphology and Segmentation During the Machining of Titanium Alloys," J. Mater. Process. Technol., **150**(1–2), pp. 124–133.
[106] Childs, T. H. C., Arrazola, P. J., Aristimuno, P., Garay, A., and Sacristan, I., 2018, "Ti6Al4 V Metal Cutting Chip Formation Experiments and Modelling Over a Wide Range of Cutting Speeds," J. Mater. Process. Technol., **255**, pp. 898–913.
[107] Melkote, S. N., Liu, R., Fernandez-Zelaia, P., and Marusich, T., 2015, "A Physically Based Constitutive Model for Simulation of Segmented Chip Formation in Orthogonal Cutting of Commercially Pure Titanium," CIRP Ann., **64**(1), pp. 65–68.
[108] Chen, G., Ren, C., Yang, X., Jin, X., and Guo, T., 2011, "Finite Element Simulation of High-Speed Machining of Titanium Alloy (Ti-6Al-4V) Based on Ductile Failure Model," Int. J. Adv. Manuf. Technol., **56**(9–12), pp. 1027–1038.
[109] Barry, J., and Byrne, G., 2002, "The Mechanisms of Chip Formation in Machining Hardened Steels," ASME J. Manuf. Sci. Eng., **124**(3), pp. 528–535.
[110] Turley, D. M., Doyle, E. D., and Ramalingam, S., 1982, "Calculation of Shear Strains in Chip Formation in Titanium," Mater. Sci. Eng., **55**(1), pp. 45–48.
[111] Siemers, C., Baeker, M., Mukherji, D., and Rösler, J., 2003, "Microstructure Evolution in Shear Bands During the Chip Formation of Ti6Al4V," Proceedings of the 10th World Titanium Conference Ti-2003, Hamburg, Germany, p. 853.
[112] Gente, A., Hoffmeister, H. W., and Evans C.J., 2001, "Chip Formation in Machining Ti6Al4V at Extremely High Cutting Speeds," CIRP Ann., **50**(1), pp. 49–52.
[113] Yadav, S., and Sagapuram, D., 2020, "In Situ Analysis of Shear Bands and Boundary Layer Formation in Metals," Proc. R. Soc. A, **476**(2234), p. 20190519.
[114] Mallock, A., 1882, "The Action of Cutting Tools," Proc. R. Soc. London, **33**(216–219), pp. 127–139.
[115] Udupa, A., Viswanathan, K., Davis, J. M., Saei, M., Mann, J. B., and Chandrasekar, S., 2019, "A Mechanochemical Route to Cutting Highly Strain-Hardening Metals," Tribol. Lett., **67**(1), p. 4.
[116] Shanley, F. R., 1946, "The Column Paradox," J. Aeronaut. Sci., **13**(12), p. 678.
[117] Shanley, F. R., 1947, "Inelastic Column Theory," J. Aeronaut. Sci., **14**(5), pp. 261–268.
[118] Udupa, A., Viswanathan, K., and Chandrasekar, S., 2020, "Pattern Formation on Free Surfaces via Plastic Buckling and Periodic Folding," Europhys. Lett., **129**(4), p. 46001.
[119] Udupa, A., Viswanathan, K., Saei, M., Mann, J. B., and Chandrasekar, S., 2018, "Material-Independent Mechanochemical Effect in the Deformation of Highly-Strain-Hardening Metals," Phys. Rev. Appl., **10**(1), p. 014009.
[120] Udupa, A., Sugihara, T., Viswanathan, K., and Chandrasekar, S., 2019, "Altering the Stability of Surface Plastic Flow via Mechanochemical Effects," Phys. Rev. Appl., **11**(1).
[121] Pugh, H. L. D., 1958, "Mechanics of the Cutting Process," Proceedings of the Conference on Technology of Engineering Manufacture, London, pp. 237–254.
[122] Hill, R., 1954, "The Mechanics of Machining: A New Approach," J. Mech. Phys. Solids, **3**(1), pp. 47–53.
[123] Hill, R., 1954, "On the Limits Set by Plastic Yielding to the Intensity of Singularities of Stress," J. Mech. Phys. Solids, **2**(4), pp. 278–285.
[124] Kudo, H., 1965, "Some New Slip-Line Solutions for Two-Dimensional Steady-State Machining," Int. J. Mech. Sci., **7**(1), pp. 43–55.
[125] Roth, R. N., 1975, "The Range of Permissible Shear Angles in Orthogonal Machining Allowing for Variable Hydrostatic Stress on the Shear Plane and Variable Friction Angle Along the Rake Face," Int. J. Mach. Tool Des. Res., **15**(3), pp. 161–177.
[126] Dewhurst, P., 1978, "On the Non-Uniqueness of the Machining Process," Proc. R. Soc. A, **360**(1703), pp. 587–610.